

Review

# Plasma-Activated Water: Physicochemical Properties, Generation Techniques, and Applications

Kiing S. Wong, Nicholas S. L. Chew, Mary Low and Ming K. Tan \* 

Department of Mechanical Engineering, School of Engineering, Monash University Malaysia,  
Bandar Sunway 47500, Malaysia

\* Correspondence: tan.ming.kwang@monash.edu

**Abstract:** Plasma-activated water (PAW) is water that has been treated with atmospheric pressure plasma. Due to the presence of reactive oxygen and nitrogen species (RONS), PAW can be used in various applications such as (1) surface disinfection and food decontamination, (2) enhancement in seed germination, and (3) enhancement in surface cooling in the nucleate boiling regime. Briefly, for surface disinfection, the reactive species in PAW can induce oxidative stress on microbes; for enhancement of seed germination, the reactive species in PAW can trigger seed germination and provide nutrients; for enhancement in surface cooling, the reactive species cause a reduction in the surface tension of PAW, facilitating the phase-change heat transfer and, quite unexpectedly, minimizing the surface oxidation. Here, we review the physicochemical properties of PAW, the three commonly used techniques (plasma jet, dielectric barrier discharge, and corona discharge) for generating atmospheric pressure plasma, and the use of PAW for the above three applications. In particular, we review the recent development of the miniaturization of the plasma generator integrated with an acoustic neutralizer to produce plasma-activated aerosols, elimination of the need for storage, and the interesting physicochemical properties of PAW that lead to cooling enhancement.

**Keywords:** plasma-activated water (PAW); plasma jet; dielectric barrier discharge; corona discharge; disinfection; germination; cooling



**Citation:** Wong, K.S.; Chew, N.S.L.; Low, M.; Tan, M.K. Plasma-Activated Water: Physicochemical Properties, Generation Techniques, and Applications. *Processes* **2023**, *11*, 2213. <https://doi.org/10.3390/pr11072213>

Academic Editor: Francesco Parrino

Received: 9 June 2023

Revised: 17 July 2023

Accepted: 19 July 2023

Published: 23 July 2023



**Copyright:** © 2023 by the authors. Licensee MDPI, Basel, Switzerland. This article is an open access article distributed under the terms and conditions of the Creative Commons Attribution (CC BY) license (<https://creativecommons.org/licenses/by/4.0/>).

## 1. Introduction

Plasma-activated water (PAW) is water that has been treated by a stream of ionized gas (plasma), which is rich in reactive species [1]. In recent years, many studies have shown that PAW can provide effective inactivation of pathogenic microbes [2,3]. Additionally, PAW also can enhance seed germination [4] and surface cooling (in the nucleate boiling regime) [5,6], as well as the anaerobic treatment of palm oil mill effluent [7]. The effectiveness of PAW in these applications is strongly dependent on the concentration of reactive species, which can be categorized into two major groups: reactive oxygen species (ROS) and reactive nitrogen species (RNS).

For application in disinfection, the ROS generated in PAW such as hydrogen peroxide, hydroxyl radical, and ozone are strong oxidizing agents and are capable of inducing oxidative stress on the microbial cell membranes. For instance, the structure and chemical bonds of the cell membrane protein of *Staphylococcus aureus* can be altered after being exposed to PAW [3]. These ROS in PAW are also capable of promoting lipid oxidation in the cell membrane [8,9]. The ROS can destroy the intramolecular bonds of peptidoglycan by removing a hydrogen atom from the peptide bond from the peptidoglycan layer that is present outside the plasma membrane of most bacteria, which can lead to cell wall breakdown, stoppage of metabolic activities, cell damage, and death [3,10–12]. For application in seed germination, on the other hand, ROS plays a role in regulating phytohormones levels, thereby triggering cell metabolism process [13]. Regulating the concentration of ROS is crucial, because excessive concentrations can induce high oxidative stress that inhibits the

germination process [4,14,15]. Similarly, RNS serve as a source of nutrition for plants and regulate cellular redox status, facilitating cell development [16].

The presence of reactive oxygen and nitrogen species (RONS) in PAW can change the physical properties of the solutions. For instance, by increasing the electrical conductivity of the PAW, surface tension can be reduced significantly, leading to higher evaporate rates (for phase-change heat transfer) and thus heat removal rates [5,6]. Here, we first discuss the physiochemical properties of the PAW (Section 2), the common techniques to produce PAW (Section 3), the applications of PAW (Section 4), and finally, the recent efforts to develop miniaturized plasma generator for directly plasma-activated aerosols on contaminated surfaces (Section 5).

## 2. Physicochemical Properties of Plasma-Activated Water

As the plasma comes into contact with water, various RONS are produced at the air–liquid interface. The generated primary reactive species then react with the water molecules and each other to form various secondary species that are crucial to the applications [17]. The generated active species can be separated into long-lifetime species such as hydrogen peroxide ( $\text{H}_2\text{O}_2$ ), ozone ( $\text{O}_3$ ), nitrite ( $\text{NO}_2^-$ ) and nitrate ( $\text{NO}_3^-$ ), which typically have a half-life of minutes to days [18,19] and short-lifetime species such as hydroxyl radicals (OH), nitric oxide (NO), and peroxyxynitrite ( $\text{ONOO}^-$ ), which typically have a half-life ranging from one nanosecond to several seconds that quickly react to create stable species [20,21]; this is the motivation to develop in situ application of plasma-activated water/aerosols (see Section 5). Here, we discuss the physical properties (Section 2.1), ROS (Section 2.2), and RNS (Section 2.3) in PAW, as well as common analytical methods for reactive species measurement (Section 2.4).

### 2.1. Physical Properties

**Density**—the density of PAW is directly proportional to the concentration of ions, as shown in Figure 1a. During the plasma treatment, various free-moving charged species and ions diffuse into the water, resulting in higher concentrations of these ions and thus an increase in density [5,6].

**Surface tension**—the surface tension of PAW decreases with the increase in electrical conductivity, as shown in Figures 1b and 2. The reduction in surface tension could be attributed to an increase in  $\text{NO}_3^-$  ions in PAW, which can interfere with the hydrogen bond of the water molecule when the  $\text{NO}_3^-$  ions are attracted to the air–liquid interface [22,23].

**pH**—the pH of PAW decreases with the increase in treatment duration, as shown in Figure 1d [24–26]. However, under an extended treatment duration, the rate of reduction in pH is reduced and subsequently reaches a steady-state where it remains constant. Despite its acidity and low pH, PAW is considered safe for application on the skin as a disinfectant. It is neither toxic nor corrosive [27]. Studies have demonstrated that when PAW is applied to mice, it can facilitate skin wound healing without causing any damage to the tissues [28,29]. Furthermore, an in vivo study conducted on mice with pancreatic cancer cells showed that PAW is non-toxic and safe for use in animals [30]. When the pH of PAW is relatively neutral, the concentration of reactive species such as  $\text{H}_2\text{O}_2$ ,  $\text{NO}_2^-$ ,  $\text{NO}_3^-$ , and  $\text{ONOO}^-$  can remain stable over time. However, at lower pH values ( $\text{pH} < 3.5$ ), the reactive species become unstable and undergo active reactions with each other, leading to an unstable concentration of reactive species [31,32]. Nonetheless, a recent study demonstrated a hybrid conservation and restoration method for PAW through low-temperature storage and pH adjustment [33]; this method can efficiently preserve the bactericidal effect of PAW for up to 10 days.

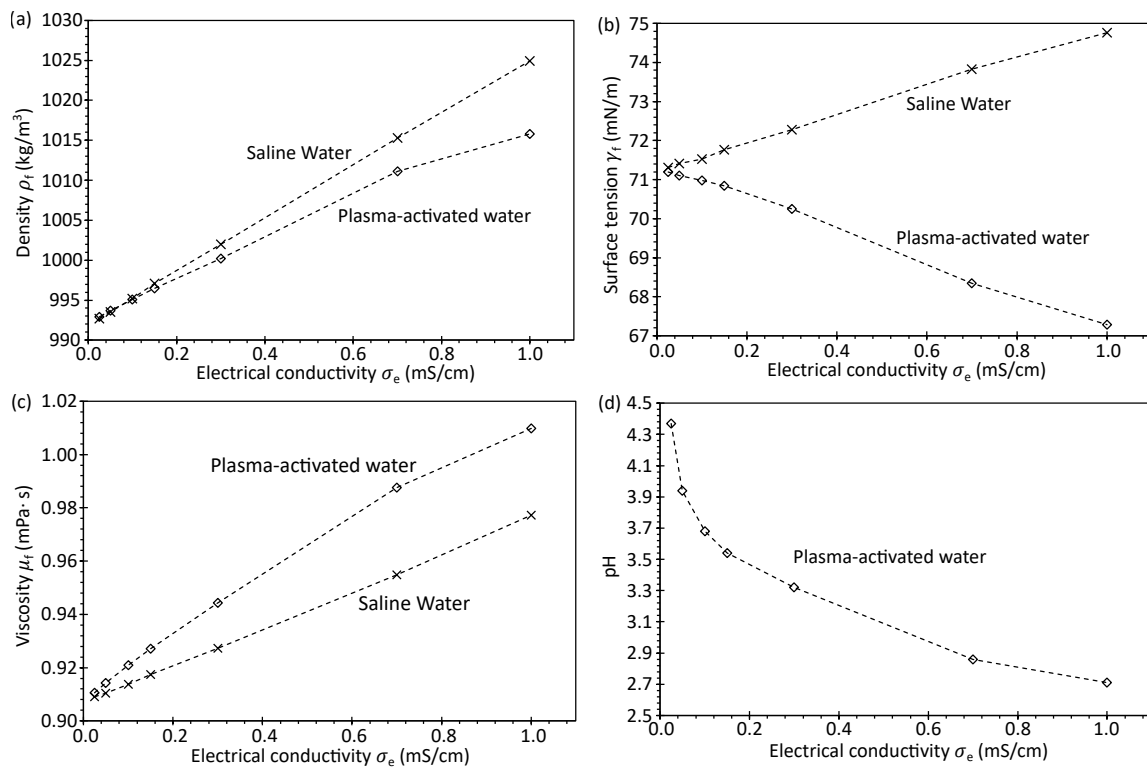


**Figure 1.** By exposing deionized water to atmospheric pressure plasma (to produce PAW), due to the dissolved and the subsequent formations of reactive species in the water, the physical properties such as (a) density, (b) surface tension, (c) viscosity, and (d) pH can be altered significantly. As can be seen here, the higher the concentration of these reactive species, the higher the electrical conductivity  $\sigma_e$  of the PAW. Note that the PAW was produced via the corona discharged plasma. From [34]. Copyright 2023 Author(s), licensed under a Creative Commons Attribution (CC BY-NC-ND 4.0) License.

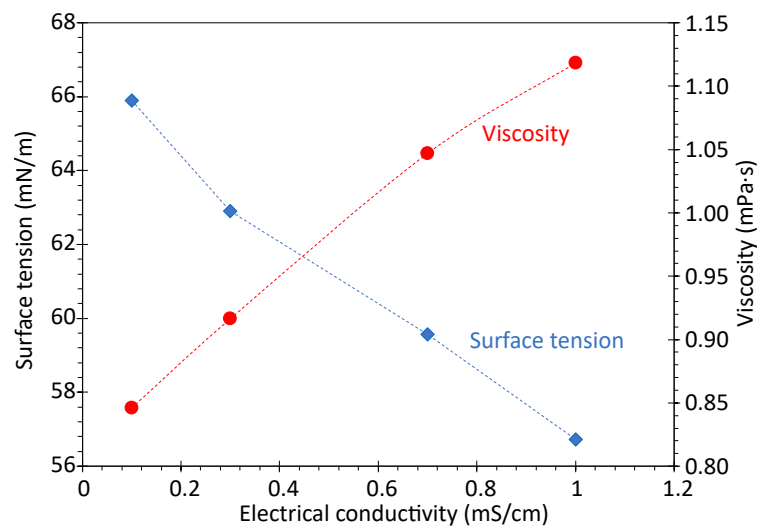


**Figure 2.** PAW produced using plasma jet (with compressed air as feeding gas) has similar characteristics to those produced using the corona discharge plasma (see Figure 1), i.e., by increasing the electrical conductivity of the solutions, the surface tension is reduced, whereas the viscosity is increased.

**Electrical conductivity**—As PAW consists of various free-moving charged species and ions due to the diffusion of reactive species into the water while being treated by plasma, the conductivity is increased. Studies have shown that the conductivity of PAW can increase

to the range of 100–500 mS/cm [25,35,36]. The electrical conductivity of PAW is one of the important indicators of the overall concentration of the reactive species and ions.

**Oxidation–reduction potential**—PAW has higher oxidation–reduction potentials. For instance, hydrogen peroxide  $\text{H}_2\text{O}_2$  is one of the important species that leads to higher oxidation–reduction potentials due to its ability to act as an oxidant or as a reductant [37]. Similarly, ROS such as hydroxyl radical OH and ozone  $\text{O}_3$ , as well as RNS such as nitrates  $\text{NO}_3^-$ , nitrites  $\text{NO}_2^-$ , and peroxyxynitrite  $\text{ONOO}^-$  also contribute to the high oxidation–reduction potential [38].

## 2.2. Reactive Oxygen Species (ROS)

**Hydroxyl radical (OH)** is the precursor of hydrogen peroxide found in PAW and is a strong oxidizing agent [39]. It has a short lifetime of approximately 200  $\mu\text{s}$  in the gas phase and only several nanoseconds in the liquid phase due to its high reactivity [40]. OH has a vital role in the formation of various reactive species especially in the gas phase (prior to their diffusion into the liquids). The concentration of the reactive species in the PAW for antimicrobial application is closely related to the concentration of the OH [41]. Due to its short lifetime, the OH found in PAW is usually from secondary reactions such as the breakdown of hydrogen peroxide and the reaction of ozone with hydrogen peroxide or hydroperoxyl radical [42].

**Hydrogen peroxide ( $\text{H}_2\text{O}_2$ )** is the most common long-lifetime species found in PAW and has an important role in antimicrobial and seed germination [4,43,44].  $\text{H}_2\text{O}_2$  is mainly generated in PAW through two pathways: (1) OH radicals generated in the gas phase combine into  $\text{H}_2\text{O}_2$  and then diffuse directly into the liquid phase and (2) OH radicals generated in the gas phase diffuse into the liquid phase and then combine to form  $\text{H}_2\text{O}_2$  [41,45].  $\text{H}_2\text{O}_2$  is capable of freely diffusing through the cell membrane without disrupting it. Hence, hydrogen peroxides that cooperate with it are able to damage and increase the permeability of the cell membrane, leading to the ease of extracellular reactive species in the PAW to invade the targeted cell [46].

**Ozone ( $\text{O}_3$ )** in an aqueous solution is a strong antimicrobial oxidizing agent that possesses one of the highest oxidation–reduction potential values among typical oxidants such as permanganate,  $\text{H}_2\text{O}_2$ , chlorine, and chlorine dioxide [47]. It is mainly generated in PAW through two pathways: (1)  $\text{O}_3$  generated in the gas phase diffuses directly into the liquid phase and (2)  $\text{O}_3$  generated in the liquid phase by plasma discharge in bubbles containing oxygen [37]. Nevertheless, a previous study indicated that the  $\text{O}_3$  concentration may be negligible in PAW due to its aggressive reactions with nitric oxide and nitrogen dioxide in the gas phase, and, also with nitrite in the liquid phase [18].

**Superoxide ( $\text{O}_2^-$ )** is yet another important ROS that is generated when water is treated with atmospheric pressure plasma. It is mainly produced from (1) the highly energetic electrons ejected by the plasma reacting with oxygen molecules, (2) OH reacting with  $\text{O}_3$ , and (3) the secondary reaction of peroxyxynitrite into  $\text{O}_2^-$  and nitric oxide. A previous study showed that  $\text{O}_2^-$  is essential for bacteria inactivation because the critical pH value for antimicrobial effects is strongly related to the acid dissociation constant between the  $\text{O}_2^-$  and hydroperoxy radicals, both of which interact and inactivate bacterial cells [48].

## 2.3. Reactive Nitrogen Species (RNS)

**Nitrites ( $\text{NO}_2^-$ )** and **nitrates ( $\text{NO}_3^-$ )** are both long lifetime species, generated as secondary products in PAW. In a low pH environment, nitrite easily degrades and protonates into  $\text{H}_2\text{O}_2$ , nitric oxide and nitrogen dioxide that are considered to be very toxic to cells [49,50].  $\text{NO}_2^-$  are produced from nitrogen oxides ( $\text{NO}_x$ ) that are generated through the reaction between nitrogen and oxygen in the gas phase during the plasma treatment [51]. When  $\text{NO}_2^-$  interact with an oxidizing agents such as  $\text{H}_2\text{O}_2$  and ozone, it can convert to  $\text{NO}_3^-$  [52]. Thus, the formation of  $\text{NO}_2^-$  and  $\text{NO}_3^-$  in PAW is accompanied by ROS, such as  $\text{H}_2\text{O}_2$ . Furthermore, the production of  $\text{NO}_2^-$  and  $\text{NO}_3^-$  in PAW is affected by the treatment conditions and type of plasma generator used [24,53].

**Nitric oxide** (NO) is a signaling molecule and can be found ubiquitously in various organisms. It has the ability to inhibit bacteria, induce apoptosis in cancer cells, and help in wound healing [54]. NO in the PAW can be formed by the dissolution of NO from the gas phase into the liquid phase or by secondary reactions in the PAW [55]. Nonetheless, due to the low solubility of NO in water and its low to moderate gas phase density, the NO found in PAW is mainly from the secondary reaction between nitrogen dioxide with atomic oxygen or  $O_3$  [56]. Recent studies indicate that NO has a short lifetime and converts into  $NO_2^-$  and  $NO_3^-$  quickly in PAW [46,57].

**Peroxynitrite** ( $ONOO^-$ ) is a strong oxidizing and nitrating agent that has an important role in disease regulation and can help combat neuro-degeneration, inflammation, diabetes, and other pathologies [58]. The formation pathways of  $ONOO^-$  are mainly from the reaction of (1) NO with  $H_2O_2$  or  $O_2^-$ , and (2)  $NO_2^-$  with  $H_2O_2$  or hydroperoxyl radicals [59,60]. As both  $NO_2^-$  and  $H_2O_2$  have a strong synergistic effect in the inactivation of microorganisms and they react to form  $ONOO^-$  in an acidic environment,  $ONOO^-$  can potentially be a crucial species in the antimicrobial properties in PAW [52].

#### 2.4. Methods to Measure Reactive Species

Two commonly used analytical techniques to measure the reactive species in PAW are electron spin resonance and UV absorption spectroscopy.

**Electron spin resonance** (ESR) can be used to detect and quantify free radicals in PAW. During measurement, the sample is subjected to horizontal magnetic and vertical microwave radiation [61]. The free radicals within the sample are excited when the frequency of the microwaves meets the resonance condition; their energy fluctuation is proportional to the magnetic field strength. To detect short-lifetime species, a spin trap reagent reacts with free radicals and forms stable spin-trapped adducts, which can be analyzed using ESR spectroscopy. Different spin-trapped reagents are used depending on the specific reactive species of interest, and the resulting spin-trapped adducts exhibit distinct ESR spectra, enabling their identification and quantification [53,62,63].

**UV absorption spectroscopy** (UV-Vis) is another technique used to quantify the reactive species by measuring the absorption of ultraviolet (UV) and visible light by the PAW. A spectrophotometer is used to emit a broad spectrum of light that includes UV and visible wavelengths. As the light passes through the sample, the reactive species absorb the light based on their characteristic absorption patterns at specific wavelengths, and the detector measures the amount of light absorbed by the sample at different wavelengths. Each reactive species has unique absorption peaks and bands at specific wavelengths. Chemical probes are often used in conjunction with UV-Vis spectroscopy to enhance the detection of specific reactive species. These probes react with the reactive species to form colorimetric or fluorogenic products that can be easily detected. Different chemical probes are used depending on the targeted reactive species [53,62,63].

### 3. Generation Techniques: Atmospheric Pressure Plasma for the Production of Plasma-Activated Water

Generally, for the production of PAW, there are three commonly use techniques to generate atmospheric pressure plasma: (1) plasma jet (Section 3.1), (2) dielectric barrier discharge (Section 3.2), and (3) corona discharge (Section 3.3).

#### 3.1. Plasma Jet

A stable and uniform plasma jet is generated when a time-varying high voltage is applied to the electrode, and the amplitude is sufficient to ionize the compressed gas that flows within the capillary tube [64], as illustrated in Figure 3. In general, the physico-chemical properties of PAW generated from the plasma jet are relied on both the physical parameters (the geometry of the setup) and the operating parameters (types of feeding gases and their flowrate, volume of treated water, electrical power, and treatment duration).

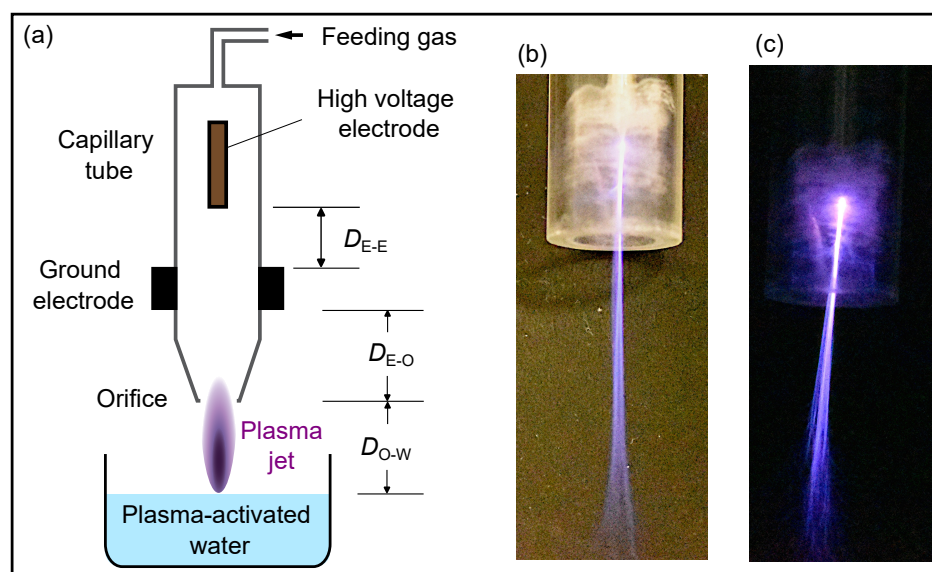


**Figure 3.** (a) Sketch illustrates the common setup to generate plasma jet for the production of PAW. Briefly, the setup consists of a supply of feeding gas, two electrodes, and a capillary tube. The electrode inside the capillary tube is connected to a high-voltage power supply, and the electrode outside the capillary tube is connected to the ground terminal. When a high voltage is applied across the electrodes, plasma is generated. The strong electric field on the surface of the dielectric tube (capillary tube) can break down the gas molecules and accelerate electrons. Images (b,c) show the typical plasma jet with nitrogen as feeding gas.

To generate a plasma jet for the efficient production of PAW, the important setup parameters are (1) the distance between the high voltage and ground electrodes  $D_{E-E}$ , (2) the distance between the ground electrode and the orifice  $D_{E-O}$ , and (3) the distance between the orifice to the liquid–air interface  $D_{O-W}$ . For the first setup parameter, the concentration of  $H_2O_2$  concentration in PAW can be controlled by adjusting the distance between the high-voltage and ground electrodes  $D_{E-E}$  [65]. This can be attributed to the increase in charge accumulation on the inner surface of the capillary tube as the distance between the electrodes is increased, facilitating the ionization process. Furthermore, the discharge volume is increased by increasing  $D_{E-E}$ , leading to higher electron densities and temperatures [66], and thus increase the rate of water evaporation (at the liquid–air interface). This allows the plasma to chemically react with the evaporated water molecules to form  $H_2O_2$  ions [67–69].

For the second setup parameter, increasing the distance between the ground electrode and the orifice  $D_{E-O}$  causes electrons to travel a longer distance before leaving the orifice, delaying electron propagation and reducing the electron density. Consequently, it interrupts the interactions of short-lifetime species and leads to lower concentrations of reactive species in the PAW [65,70]. For the third setup parameter, the increase in distance between the orifice and the liquid–air interface  $D_{O-W}$  decreases the electrical conductivity, oxidation–reduction potential, and reactive species concentrations in PAW [69]. Particularly, with the increase in  $D_{O-W}$ , the production rate of  $H_2O_2$  in the PAW is reduced; however, the production of nitrogen species is not affected [67]. This can be attributed to the decrease in the electron temperature and the increase in the electron density, i.e., lower electron temperatures reduce the evaporation of water molecules and hence decrease the formation rate of  $H_2O_2$ , whereas higher electron densities increase the collision rate between heavy neutrals (nitrogen molecules), exciting them into first metastable states, which leads to the formation of nitrogen species [67,71].

The operating parameters can also have significant effects on the concentration of reactive species in PAW. These operating parameters are the type of feeding gases and their flowrate, volume of treated water, electrical power, and treatment duration. The feeding

gas refers to the gas that sustains the plasma, while the surrounding gas is the ambient gas outside the orifice. The most commonly used feeding gases are argon, helium, and air. The plasma jet generated with helium has a lower discharge current, longer plasma length, and higher levels of O and  $N_2^+$  ions, whereas the plasma jet generated with argon has a shorter jet length, higher discharge current, and higher levels of OH and nitrogen ions. Helium metastable energy is capable of ionizing and exciting nitrogen into  $N_2^+$  and OH, while the energy of argon is insufficient to ionize nitrogen [72]. PAW produced using plasma jet with argon has the lowest electrical conductivity and  $NO_3^-$  concentration, but the highest  $H_2O_2$  concentration and pH values. Conversely, PAW produced using plasma jet with air has the highest electrical conductivity and  $NO_3^-$  concentration, but the lowest  $H_2O_2$  concentration and pH value. This is because plasma jet with argon can generate higher OH and nitrogen emissions, whereas plasma jet with air can generate high nitrogen but low OH emissions [73]. Mixing different feeding gases can further alter the reactive species concentrations. For instance, using the mixture of nitrogen and argon gases, the concentration of  $NO_2^-$  and  $NO_3^-$  ions can be increased, but the concentration of  $H_2O_2$  is decreased in PAW. On the other hand, using the mixture of oxygen and argon gases, both the concentration of  $H_2O_2$  and  $NO_3^-$  ions can be increased. The oxygen feeding gas increases the oxidizing substances like O and  $O_3$ , which oxidize the gaseous NO and  $NO_2^-$  ions, whereas the nitrogen feeding gas has a higher electron density that increases the interaction of active electron, hydrogen atoms, and hydroxyl radical to form RNS [74–77].

Another important operating parameter is the flowrate of feeding gas. For instance, for the plasma jet with argon, higher flowrates of argon gas can produce higher concentrations of  $H_2O_2$  in PAW [65]. This can be attributed to the residual humidity in commercial argon gas, which increases with the flow rate, leading to an increase in the level of water molecules in the discharge region, where they can dissociate into OH. Furthermore, higher flowrates can increase the transmission of electrical energy to gas molecules and the transportation of OH to the target solution, reducing the hydroxyl quenching reactions with the ambient air. Nonetheless, excessive flowrate of feeding gas can decrease the electron excitation temperature and  $H_2O_2$  concentration [78,79]. The concentration of reactive species in PAW is also influenced by the volume of treated water. For instance, the concentration of  $H_2O_2$  in PAW treated by kHz plasma jet increases linearly regardless of the treated volume [76]. However, concentrations of  $NO_2^-$  and  $NO_3^-$  reach saturation at the smaller volume (25 mL), but not observed in larger treated volumes (125 mL and 200 mL), which was attributed to the saturation effect likely due to recombination processes involving the high concentration of  $H_2O_2$  [76].

The electrical power of plasma jet is another important operating parameter. Higher electrical powers can increase the electrical conductivity and oxidation–reduction potential, but decrease the pH value of the PAW. This is because higher electrical powers can increase the electric field within the plasma jet, inducing a stronger intensity, longer plasma length and higher electron density [72,80–82]. In addition, the physicochemical properties of PAW generated by plasma jet also greatly influence by treatment duration. Studies reported that the electrical conductivity, oxidation–reduction potential and the concentration of reactive species in PAW increase linearly with the increase in treatment duration with a range of 0 to 20 min of treatment duration [69,74,83,84]. Specifically, the conductivity of PAW reaches 1500  $\mu S/cm$  and the concentration of  $H_2O_2$  and formation of  $NO_2^-$  and  $NO_3^-$  reaches 70  $\mu M$  and 15 mM, respectively, after 15 min of plasma jet treatment duration [69]. However, this trend is no longer obtainable if the treatment duration extended beyond the optimum duration. Zhou et al., demonstrated that the concentration of ROS increases linearly regardless the treatment duration, whereas the concentration of RNS reaches saturation after 20 min of treatment duration [52]. Similar to the volume of treated liquid, this saturation effect is likely due to recombination processes involving the high concentration of  $H_2O_2$  present in the smaller volume.

### 3.2. Dielectric Barrier Discharge

Unlike the plasma jet, dielectric barrier discharge can generate atmospheric pressure plasma directly in ambient air without the need to supply feeding gas, as illustrated in Figure 4. Thus, the dielectric barrier discharge is scalable for the mass production of PAW [85–88]. For dielectric barrier discharge, the important setup parameters that have significant effects on the concentration of reactive species in PAW are (1) material for the electrode, (2) material for the dielectric layer/substrate, and (3) distance between the electrodes, and (4) thickness of the dielectric layer/substrate. For the first setup parameter, the electrode's material, when comparing silver, stainless steel, and brass electrodes, due to the strong oxidation of silver, dielectric barrier discharge with silver electrodes can lead to higher concentrations of reactive species emission and  $\text{NO}_3^-$  concentration in PAW, but lower concentrations of  $\text{O}_3$  [89].

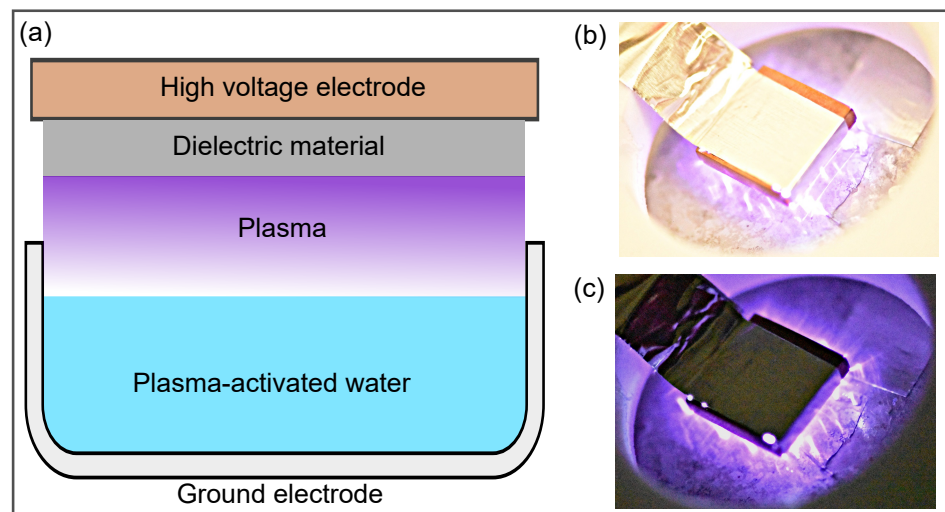


**Figure 4.** (a) Sketch illustrates the common setup to generate dielectric barrier discharge for the production of PAW. Briefly, the setup consists of electrodes and dielectric material. When a high voltage is applied across the electrodes, the dielectric material (between the electrodes) accumulates charges on its surface, creating an electric field that counteracts the external electric field and limits current flow, thus preventing sparks or arcs. The high electric field between the electrodes breaks down gas molecules, forming plasma. Images (b,c) show the typical dielectric barrier discharge where glass substrate was used as the dielectric barrier.

For the second setup parameter on the dielectric layer/substrate's material, alumina, which has a high thermal conductivity and surface roughness, can promote the generation of filaments and facilitate heat dissipation. Quartz, on the other hand, can sustain a high electrical potential applied between the electrodes, leading to higher gas ionization rates, thus increasing the concentration of reactive species in PAW [90]. For the third setup parameter on the distance between the electrodes, due to the accumulation of electrons near the dielectric barrier, decreasing the distance can lead to higher concentrations of reactive species [91], giving rise to the high microbial inactivation [92–94]. For the fourth setup parameter, the thickness of the dielectric layer/substrate, thicker dielectric layer/substrates can sustain higher electrical potential between the electrodes, leading to a higher density of micro-discharges with a uniform spatial distribution in the entire discharge region [90].

The important operating parameters that have significant effects on the concentration of reactive species in PAW are: (1) electrical power, (2) treatment duration, and (3) surrounding gas. For electrical power, the important factors are the applied frequency, voltage, current, and duty cycle [95–97]. For instance, Gao et al. [95] reported that by increasing the electrical power from 0 to 160 W, the concentration of OH can be increased from 0 to 4 mmol/L,  $\text{H}_2\text{O}_2$  can be increased from 0 to 100 mg/L,  $\text{NO}_3^-$  can be increased from 1 to 225 mg/L, and,  $\text{NH}_4$  can be increased from 0 to 1.5 mg/L in the PAW. This increase can

be attributed to an increase in energy density which enhances the rate of gas ionization [98]. An earlier study also demonstrated that changing the frequency and duty cycle of applied power can alter the efficiency of plasma-activated persulfate for sulfamethoxazole (SMZ) degradation in water [99]; an optimal duty cycle of 75% has shown the best SMZ degradation efficiency and the SMZ degradation efficiency increased from 77.3% to 89.2% when the discharge frequency was tuned from 150 Hz to 200 Hz. For the second operating parameter, longer treatment duration can lead to higher concentrations of reactive species. For instance, the concentration of  $\text{NO}_2^-$  and  $\text{NO}_3^-$  in the PAW can be increased from 0 to 6.96 mg/L and 0 to 111.31 mg/L, respectively, after 60 min of treatment [100]. A separate study also showed that the concentration of  $\text{O}_3$  and  $\text{H}_2\text{O}_2$  in the PAW can be increased from 0 to 225 mg/L and 0 to 100 mg/L, respectively, after 12 min of treatment [101]. For the third operating parameter, a surrounding gas such as helium can alter the breakdown voltage, effective capacity, micro-discharge filaments, electron density, and surface charges, as compared to ambient air [102,103].

### 3.3. Corona Discharge

Compared to plasma jet and dielectric barrier discharge, corona discharge is simple and relatively easy to set up and operate [104]. The important setup parameters are (1) configurations of the electrodes and (2) geometry and material of the electrodes. The common configurations of the electrodes are: Configuration-A, Configuration-B, and Configuration-C, as illustrated in Figure 5a–c respectively. For Configuration-A (also known as liquid discharge), both electrodes are submerged in water and it can produce higher  $\text{H}_2\text{O}_2$  concentrations in the treated water. For Configuration-B (also known as gas discharge), the gas ionization takes place in the gaseous state and the generated reactive species are then dissolved into the liquid. Configuration-C (a hybrid gas–liquid discharge) can generate electrical discharge above and in the water concurrently; this enhances the production of reactive species through diffusion and direct interaction with water [105,106]. Corona discharge similar to plasma jet (known as cometary discharge) can be produced by arranging two needle electrodes, as shown in Figure 5d [107,108]. This plasma plume can be sustained without the feeding gas.

For the geometry of the electrodes, small radii of curvature are important for generation of high localized electric field strength. Generally, metal is preferable for the electrode material owing to its good electrical conductivity. However, a highly localized electric field focusing at the tip of metal electrodes and interaction of the metal with reactive species always causes erosion, which will deteriorate the operating lifetime [109,110]. An electrode material with a higher erosion rate (such as tungsten) can generate more ions in a liquid, increasing the electrical conductivity of PAW [109]. Additionally, due to the different degrees of sharpness and brittleness of the materials, tungsten and carbon electrodes required lower discharge currents as compared to aluminum, copper, and silver electrodes [111].

The important operating parameters are (1) electrical power and (2) treatment duration. For instance, the production of OH in the gaseous state is increased by increasing the electrical power [112]. The electrical power is directly proportional to the discharge power, i.e., higher discharge powers can produce PAW with higher electrical conductivities and concentrations of  $\text{H}_2\text{O}_2$  [113]. This can be attributed to the higher electric field and ionic wind velocity between the electrodes, leading to the increase in the formation of reactive species in the gaseous state as well as the transport of these reactive species to the liquid–air interface. As the density of these reactive species increases at the liquid–air interface, it accelerates the diffusion rate of reactive species into liquid [113–116]. Increasing treatment duration also increases the concentration of reactive species. For instance, the electrical conductivity of distilled water can be increased from 7.5 to 200  $\mu\text{S}/\text{cm}$  after 30 min of treatment, and  $\text{H}_2\text{O}_2$  concentration is increased from 0 to 60 mg/L after 14 min treatment [117].

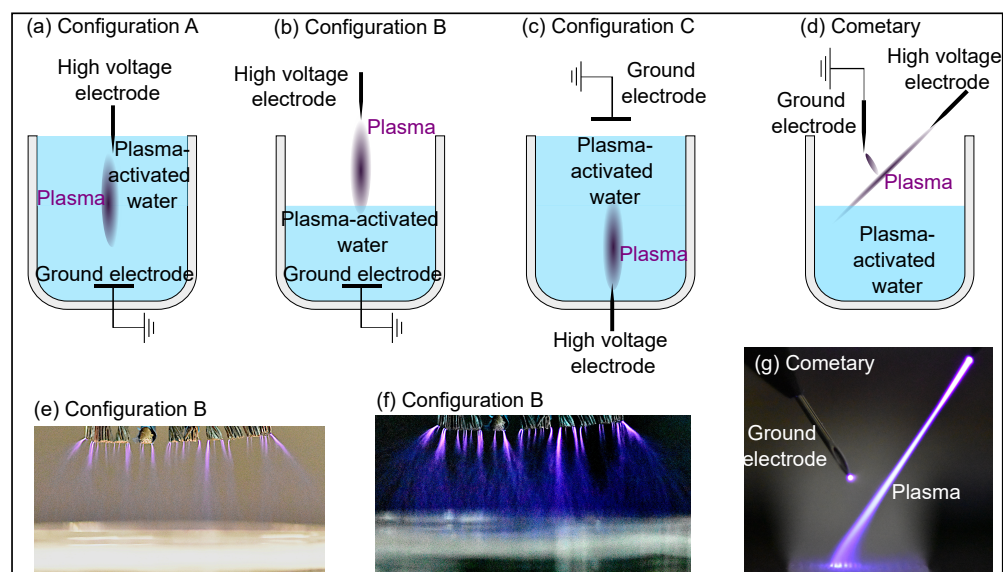


**Figure 5.** Sketches illustrate the common configurations to generate corona discharge for the production of PAW. (a) Configuration-A, both electrodes are submerged in water; (b) Configuration-B, the high voltage electrode is above and the ground electrode is submerged in water; (c) Configuration-C, the ground electrode is above and the high voltage electrode is submerged in water; (d) Cometary, both electrodes are above water. Briefly, when a high voltage is applied across electrodes, the electric field strength near the electrode with a smaller radius of curvature (such as a sharp needle) increases significantly. The gas in surrounding the sharp needle is excited by the high electric field strength, breaking down into electrons and ions and forming plasma. Images (e,f) show the generation of atmospheric pressure plasma based on Configuration-B, where the high voltage electrodes consist of copper wire strands; image (g) shows the cometary discharge plasma.

## 4. Applications of Plasma-Activated Water

### 4.1. Disinfection and Decontamination

Due to the presence of various reactive species in PAW, the effects of these reactive species on microorganisms such as planktonic bacteria, biofilms, molds, fungi, and viruses have been conducted, as summarized in Table 1. For instance, in vitro study of PAW on planktonic bacteria such as *Aeromonas hydrophila*, *Enterobacter aerogenes*, *Escherichia coli*, *Hafnia alvei*, *Listeria innocua*, *Leuconostoc mesenteroides*, *Listeria monocytogenes*, *Pseudomonas deceptionensis*, *Pseudomonas fluorescens*, *Staphylococcus aureus*, *Staphylococcus epidermidis*, *Shewanella putrefaciens*, and *Salmonella Typhimurium*, have been demonstrated to be an effective technique for bacterial inactivation. Additionally, PAW is also effective at inactivating fungus spores, i.e., 75% and 85% reductions in *Aspergillus flavus* and *Aspergillus brasiliensis* spores can be observed after a 24 h and 30 min exposure to the PAW [118,119]. Viruses and bacteriophages such as the Escherichia virus T4,  $\phi$ X174 bacteriophage, Escherichia virus MS2, and Newcastle disease virus (NDV) can be also inactivated effectively after exposed to PAW. For instance, after being exposed to PAW, the morphology and structure of the DNA and RNA in the Newcastle disease virus were observed to be altered and damaged [120]. More recently, due to the COVID-19 outbreak, studies have been conducted on the use of PAW to inactivate the spike protein in the receptor-binding domain that is crucial during the infection process of the SARS-CoV-2 virus [121–123]. Their results showed that PAW can be used as an effective disinfectant to stop the infectious properties of SARS-CoV-2 through the inactivation of the spike protein present in its receptor-binding domain [122].

On bacterial inactivation, the effect of PAW on Gram positive bacteria was not as significant compared to Gram negative bacteria. This can be attributed to their cell structure, as the Gram positive bacteria have thicker cell walls [80]. Furthermore, the type of cell community can also affect the antimicrobial efficiency using PAW. For instance, biofilms are more resistant to PAW as compared to planktonic cells; this is because, on the biofilms, the

bacteria attach to each other and secrete an extracellular matrix that increases their resilience to stress [124]. Molds and yeast are generally more resilient towards PAW as compared to bacteria; this is because molds/yeast belong to the eukaryotes cell group that is equipped with a complete cell membrane for added protection to their nucleic acids [125]. The cell wall of fungus is also equipped with polysaccharides that form a complex capsule structure which contributes to a thicker cell wall and added protection to the cell [126].

The effectiveness of using PAW for decontamination of fresh produces such as lettuce, mung bean, shiitake mushroom, fresh-cut apples, fresh-cut pears, and meat such as chicken breast, beef mackerel cubes, and shrimps have also been studied extensively, as summarized in Table 2. Additionally, processed food such as bean curd and rice cake have been studied. As exposing foods to PAW cause minimal changes to these foods, its application in the food industry such as areas like decontamination, meat curing and the curtailment of pesticide residues has been investigated. In the case of microbial inactivation, the type of surface texture (of the foods) where microbes are attached has a significant effect on the effectiveness of the PAW. For instance, foods with rough surfaces can reduce the effectiveness of PAW, this is due to the inability of reactive species to penetrate those areas effectively [127]. A further study on using PAW to inactivate *E. aerogenes* attached on surfaces such as glass, grapes, limes, tomatoes, and spine gourd showed a similar finding in that the effectiveness of PAW is reduced when the surface roughness is increased [128]. The reactive species such as hydrogen peroxide, nitrite and nitrate of PAW used in the experiments listed in Tables 1 and 2 have concentration range around 0–900  $\mu\text{M}$ , 0–500 mM and 0–800 mM, respectively, while the volume of PAW used is in the  $10^{-3}$ – $10^0$  L range.

**Table 1.** Table summarizes the in vitro studies of the effectiveness of PAW for antimicrobial inactivation on contaminated surfaces. PAW was produced using different techniques, surrounding gas and treatment duration  $t_{\text{PAW}}$ ; as discussed above, the technique, surrounding gas,  $t_{\text{PAW}}$  and can affect the concentration of reactive species in PAW. The PAW was then applied on the microbe community at specific (antimicrobial inactivation) treatment duration  $t_e$ , to achieve the desired reduction. DBD is referred to dielectric barrier discharge.

Technique	$t_{\text{PAW}}$	Microbe Community	$t_e$	Microbe	Reduction
Corona; Air	60 min	Biofilm	30 min	<i>S. aureus</i> [129]	4.74 log CFU/mL
DBD; Air	20 min	Fungus spores	24 h	<i>A. flavus</i> [118]	0.6 log CFU/mL
DBD; NO	10 s	Planktonic	5 min	<i>E. coli</i> O157:H7 [130]	3.10 log CFU/mL
	5 min	Planktonic	10 s	<i>L. monocytogenes</i> [130]	4.13 log CFU/mL
DBD; Ar with 1% Air	2 min	Bacteriophages	1 h	<i>E. virus</i> MS2 [131]	~11 log PFU/mL
				<i>E. virus</i> T4 [131]	>11 log PFU/mL
				$\phi\text{X174}$ bacteriophage [131]	>10 log PFU/mL
DBD; He with 1% O <sub>2</sub>	30 min	Planktonic	30 min	<i>L. monocytogenes</i> [124]	5.3 log CFU/mL
		Biofilm		<i>L. monocytogenes</i> [124]	3.2 log CFU/mL
		Planktonic		<i>S. Typhimurium</i> [124]	5.8 log CFU/mL
		Biofilm		<i>S. Typhimurium</i> [124]	3.9 log CFU/mL
Gliding arc; Humid air	5 min	On stainless steel	30 min	<i>H. alvei</i> [132]	5.36 log CFU/mL
				<i>L. mesenteroides</i> [132]	4.69 log CFU/mL
				<i>S. cerevisiae</i> [132]	3.07 log CFU/mL
Plasma jet; Air	60 s	Planktonic	6 min	<i>E. coli</i> O157:H7 [133]	3.7 log CFU/mL
	60 s	Planktonic	6 min	<i>S. aureus</i> [133]	2.3 log CFU/mL
	90 s	Planktonic	10 min	<i>P. deceptionensis</i> CM2 [134]	5 log CFU/mL
	3 min	Fungus spores	30 min	<i>A. brasiliensis</i> [119]	0.82 log CFU/mL
	5 min	Biofilm	5 min	<i>P. fluorescens</i> [135]	6 log CFU/mL
	5 min	Planktonic	10 min	<i>E. aerogenes</i> [128]	1.92 log CFU/mL
	5 min	Planktonic	0.5–24 h	<i>A. hydrophila</i> [80]	>7.12 log CFU/mL
	5 min	Planktonic	0.5–24 h	<i>E. coli</i> [80]	>6.79 log CFU/mL
	5 min	Planktonic	0.5–24 h	<i>L. innocua</i> [80]	>6.15 log CFU/mL
	5 min	Planktonic	0.5–24 h	<i>P. fluorescens</i> [80]	>6.86 log CFU/mL
	5 min	Planktonic	0.5–24 h	<i>S. aureus</i> [80]	>4.52 log CFU/mL
5 min	Planktonic	0.5–24 h	<i>S. putrefaciens</i> [80]	>7.06 log CFU/mL	

**Table 2.** Table summarizes the effectiveness of PAW for antimicrobial inactivation on contaminated foods. PAW was produced using different techniques, surrounding gas and treatment duration  $t_{PAW}$ ; as discussed above, the technique, surrounding gas,  $t_{PAW}$  and can affect the concentration of reactive species in PAW. The PAW was then applied on foods at specific (antimicrobial inactivation) treatment duration  $t_e$ , to achieve the desired reduction. DBD is referred to dielectric barrier discharge.

Technique	$t_{PAW}$	Food	$t_e$	Microbe	Reduction
DBD; Air	10 min	Fresh shrimp	9 days	Natural microflora [136]	1.32 log CFU/g
	10 min	Lettuce	5 min	<i>L. innocua</i> [137]	2.4 log CFU/g
	10 min	Lettuce	5 min	<i>P. fluorescens</i> [137]	>6 log CFU/g
	20 min	Chicken breast	20 min	<i>S. aureus</i> [138]	2.09 log CFU/g (MRSA)
	20 min	Chicken breast	20 min	<i>S. aureus</i> [138]	2.29 log CFU/g (MSSA)
	20 min	Rice cake	20 min	<i>E. coli</i> O157:H7 [139]	2.01 log CFU/g
	20 min	Rice cake	20 min	<i>L. monocytogenes</i> [139]	2.02 log CFU/g
	20 min	Rice cake	20 min	<i>S. typhimurium</i> [139]	2.08 log CFU/g
	20 min	Rice cake	20 min	<i>C. albicans</i> [139]	1 log CFU/g
	20 min	Rice cake	20 min	<i>P. chrysogenum</i> [139]	1.97 log CFU/g
Plasma jet; Air	30 s	Sprouts	30 mins	Natural microflora [140]	2.32 log CFU/g (bacteria)
	30 s	Sprouts	30 mins	Natural microflora [140]	2.84 log CFU/g (yeast/moulds)
	60 s	Beef	until frozen	Natural microflora [141]	1.98 log CFU/g (fungus/yeast)
	90 s	Bean Curd	30 min	Natural microflora [142]	1.26 log (bacteria)
	90 s	Bean Curd	30 min	Natural microflora [142]	0.91 log (yeast/molds)
	10 min	Apple	5 min	Natural microflora [143]	1.05 log CFU/g (bacteria)
	10 min	Apple	5 min	Natural microflora [143]	0.64 log CFU/g (molds)
	10 min	Apple	5 min	Natural microflora [143]	1.04 log CFU/g (yeasts)
	10 min	Bean curd	24 h	<i>E. coli</i> O157:H7 [144]	>2 log CFU/g
	10 min	Bean curd	24 h	<i>L. monocytogenes</i> [144]	~0.5 log CFU/g
	10 min	Bean curd	24 h	<i>S. enteritidis</i> [144]	>2 log CFU/g
	10 min	Bean curd	24 h	<i>S. typhimurium</i> [144]	>2 log CFU/g
	15 min	Fresh mackerel	30 min	<i>P. fluorescens</i> [145]	0.4 log CFU/g
	20 min	Mushroom	20 min	Natural microflora [146]	>1 log CFU/g
	20 min	Shell eggs	1 min	<i>S. enteritidis</i> [147]	>4 log CFU/egg
	30 min	Kiwifruit	8 days	<i>S. aureus</i> [148]	1.8 log CFU/g
60 min	Chicken breast	12 min	<i>P. deceptionensis</i> CM2 [149]	1.05 log CFU/g	

#### 4.2. Enhancement in Seed Germination

Enhancing seed germination is critical for increasing agricultural productivity, as it is a key factor in determining crop yield frequency and growth rate, which are essential for ensuring food availability [150,151]. The seed germination process involves three stages: water absorption to initiate metabolism, biological metabolism process, and termination upon radicle protrusion [152–154]. Water absorption and seed biological metabolism processes are important for increasing seed germination rate. Increasing the water absorption rate occurs mainly via physical mechanisms. Common techniques are: (1) increase the temperature [155–157], (2) increase the hydrostatic pressure [158,159], and (3) exposure to ultrasound [4,160–163]. On the other hand, increasing seed metabolism occurs mainly via chemical and biological mechanisms. Common techniques are chemical [164–168] and exogenous phytohormone [169–172] treatments for embryo development. Nonetheless, these techniques can create risks of byproduct contamination during the seed germination process and harm the environment.

PAW contains a high concentration of reactive species, which can enhance biological reactions. The effectiveness of PAW to increase germination is depended on the concentrations of ROS and RNS, as illustrated in Figure 6. The ROS act as signaling hubs, triggering transduction events in cellular responses related to seed germination, whereas the RNS are fundamental in plant nutrition, regulating cellular redox status and the synthesis of amino acid, proteins and chlorophyll [13,16,173,174]. For instance, PAW produced by plasma jet with argon–oxygen feeding gas can increase wheat seed germination process, achieving a 100% germination rate for treated seeds as compared to 97% for seeds without treatment [175]; PAW produced by plasma jet with air feeding gas can increase the pea seed germination by 37% [176]; PAW produced by dielectric barrier discharge with argon–nitrogen–oxygen surrounding gas can increase the *Lactuca sativa* L. seeds germination potential by 117% [177]. Nonetheless, not all reactive species in high concentrations are

favorable for enhancing seed germination. For instance, excessive concentration of ROS can lead to high abiotic stress and thus affect seed viability [4,14,15].

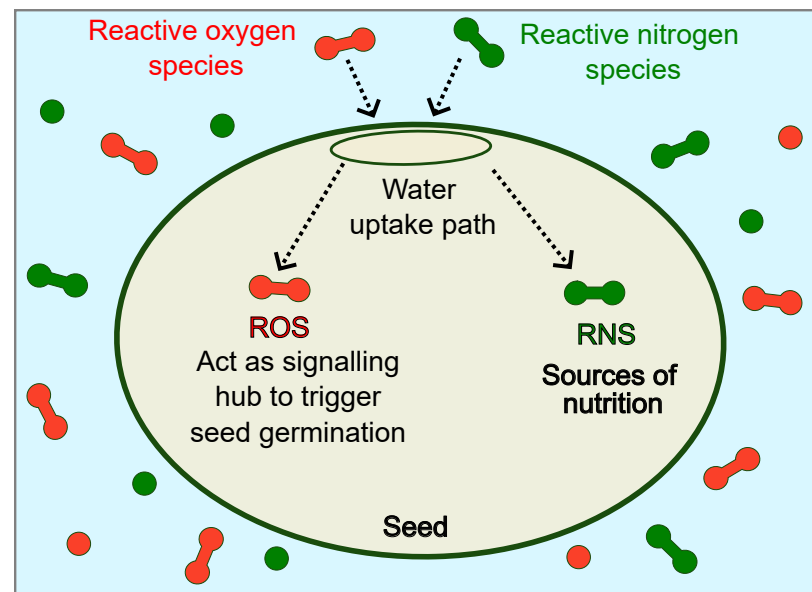


**Figure 6.** The sketch illustrates the concept of the use of PAW to enhance seed germination. ROS can act as a signaling hub to trigger the biological metabolism process during germination and RNS can act as a primary source of nutrition.

#### 4.3. Enhancement in Surface Cooling and Reduction in Surface Oxidation

Due to the presence of reactive species in PAW, the physical properties of the solutions can be altered significantly by increasing the concentrations of these reactive species, i.e., by prolonging the treatment duration such as to increase the electrical conductivity of the solutions. As can be seen in Figure 1, by increasing the electrical conductivity of PAW, the density and viscosity are increased, whereas the surface tension is reduced [34]. A similar trend was reported by Ekanayake et al. [178,179], in which they observed higher evaporation rates for seawater treated with atmospheric pressure plasma. By exploiting this interesting change in the surface tension of PAW for application in surface cooling in the nucleate boiling regime (phase-change heat transfer), Low et al. reported an increase in droplet evaporation rate (using PAW with electrical conductivity  $\sigma_e \approx 1.4$  mS/cm) by up to 40% as compared to deionized water ( $\sigma_e \approx 0.002$  mS/cm). Additionally, in the nucleate and transition boiling regimes (approximately 130–150 °C), up to 220% enhancement of the reduction in surface temperature, can be obtained by using PAW as compared to deionized water [5]. Similar enhancement in surface cooling can also be obtained for the pool cooling system, i.e., up to 66% increase in pool evaporation rate by using PAW as compared to deionized water can be achieved [6]. Peculiarly, when applying the concept on a steady-state, phase-change heat transfer cooling system that operates in the nucleation boiling regime, with the PAW ( $\sigma_e \approx 1.4$  mS/cm), they observed that not only the heat transfer coefficient can be increased by up to 73%, but the surface oxidation (after a 5 h operation) of the heat source (a copper material) is also reduced (see Figure 7) in comparison to deionized water ( $\sigma_e \approx 0.002$  mS/cm) [6]. Further studies on the effects of PAW aging on the cooling performance and the role of reactive species in altering its physical properties are needed; an earlier study showed that the stability of PAW can be maintained for up to 2 weeks by considering high reduction potential metals during the treatment [180].

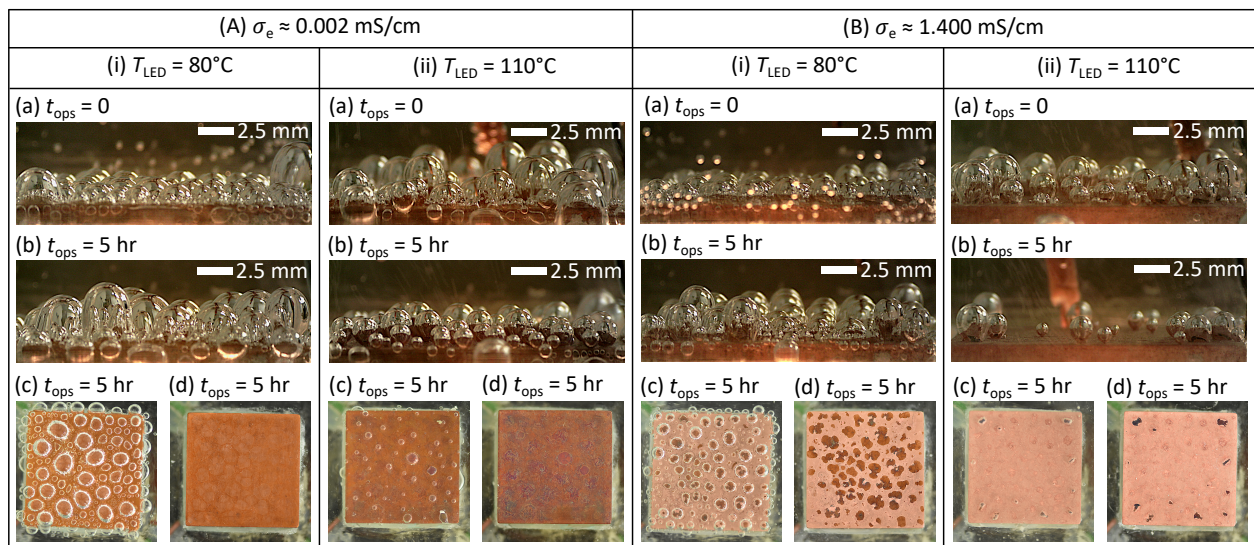


**Figure 7.** By using PAW ( $\sigma_e \approx 1.4$  mS/cm) as coolant atop the heat source (a copper material) at the steady-state surface temperature of  $110^\circ\text{C}$ , after 5 h of continuous operation, only a small fraction of copper oxides were formed on the heat source surface (B-ii-d), as compared to using deionized water ( $\sigma_e \approx 0.00$  mS/cm), where the entire surface of the heat source was oxidized (A-ii-d). From [6]. Copyright 2023 Author(s), licensed under a Creative Commons Attribution (CC BY-NC-ND 4.0) License.

### 5. Miniaturization for In Situ Generation of Plasma-Activated Aerosols

Although studies have demonstrated the effectiveness of PAW for application in surface disinfection, commercial products based on PAW are limited. This can be attributed to the challenge of making the plasma system portable by miniaturizing the plasma generator such that the PAW can be applied directly on the contaminated surfaces without the need for storage. As highlighted above, proper storage of PAW at lower temperatures is important to ensure no significant degradation of the reactive species in PAW. For instance, the effectiveness of microbial inactivation can be reduced by up to 20% and 80% when the PAW is stored at  $-80^\circ\text{C}$  and  $25^\circ\text{C}$ , respectively, for 30 days [24]. As such, there is a need to develop an integrated miniaturized plasma generator and portable nebulizer for the in situ generation of plasma-activated aerosols that can be applied directly on contaminated surfaces.

The first such system was reported by Wong et al. [181]. In their study, the plasma generator was based on the cometary discharge plasma (Figure 5d), whereas the nebulizer was based on surface acoustic wave device. By spraying the plasma-activated aerosols directly on the contaminated surfaces with *E. coli*, they obtained a percentage reduction of up to 96%. To further miniaturize the plasma generator, a nanoscale plasma generator was developed [182]. Briefly, zinc oxide nanorod carpets coated with aluminum that mimic a conglomeration of nanoneedles were used to generate plasma (see Figure 8), leading to a considerable increase in the reactive species in the plasma-activated aerosols. Although the in situ production of plasma-activated aerosols via the nanoscale plasma generator is a promising technique, it is challenging to deposit plasma-activated aerosols onto a specific contamination area. To address this limitation, DC electro spray can be used to generate plasma-activated aerosols; due to the strong electric field, these finer plasma-activated aerosols can be deposited on the contaminated surface [34].

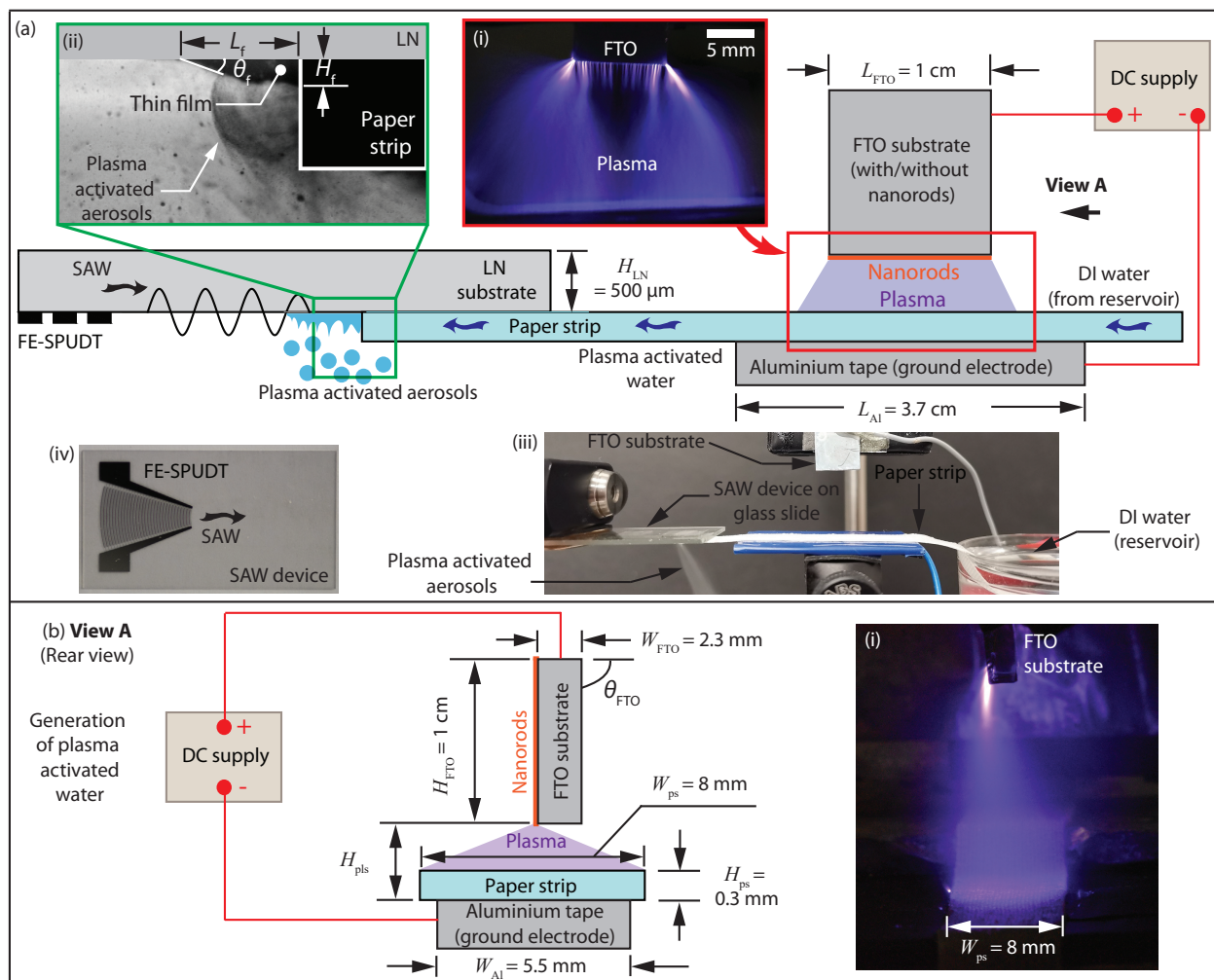


**Figure 8.** (a) Sketch illustrates the concept of an integrated nanoscale plasma generator and a portable acoustic nebulizer. Briefly, zinc oxide nanorods coated with a thin layer of aluminum were used to generate atmospheric pressure plasma (a-i) to treat the water transported within the paper strip (a-iii). When the PAW reaches the surface of the lithium niobate (LN) substrate (a-iv), due to the high surface acceleration, the liquid film destabilizes and produces plasma-activated aerosols (a-ii). (b) The rear view of the nanoscale plasma generator and (b-i) the plasma above the paper strip. From [182]. Copyright 2022 Author(s), licensed under a Creative Commons Attribution (CC BY 4.0) License.

## 6. Conclusions

PAW is an up-and-coming technology that can be used in applications such as antimicrobial activity, enhancement of seed germination, and improvement of surface cooling in the nucleate boiling regime. This is mainly attributed to the unique physicochemical properties and biochemical activities that it possesses after being treated with atmospheric pressure plasma. Here, in the first part of this review, we discussed the physicochemical properties of PAW and highlighted the common RONS in PAW that are responsible for the above three applications. Given that different techniques to generate the atmospheric pressure plasma have significant impact on the concentrations of the RONS in PAW, in the second part, we discussed the three commonly used techniques (plasma jet, dielectric barrier discharge, and corona discharge) to generate atmospheric pressure plasma. Finally, in the third part, we discussed the recent development in the use of PAW for the above three applications, such as the recently demonstrated concept of an integrated nanoscale plasma generator and acoustic nebulizer; this integrated portable system not only enables the in situ production of PAW, but also the generation of plasma-activated aerosols that can deposit directly on contaminated surfaces. While PAW has demonstrated effectiveness in

these applications, a thorough safety assessment of long-term usage must be conducted before its application in the food or biomedical industries.

**Funding:** This research received no external funding.

**Data Availability Statement:** Data sharing is not applicable to this article as no new data were created or analyzed in this study.

**Conflicts of Interest:** The authors declare no conflict of interest.

## References

1. Zhao, Y.M.; Patange, A.; Sun, D.W.; Tiwari, B. Plasma-activated water: Physicochemical properties, microbial inactivation mechanisms, factors influencing antimicrobial effectiveness, and applications in the food industry. *Compr. Rev. Food Sci. Food Saf.* **2020**, *19*, 3951–3979. [[CrossRef](#)]
2. Qi, Z.; Tian, E.; Song, Y.; Sosnin, E.A.; Skakun, V.S.; Li, T.; Xia, Y.; Zhao, Y.; Lin, X.; Liu, D. Inactivation of *Shewanella putrefaciens* by Plasma Activated Water. *Plasma Chem. Plasma Process.* **2018**, *38*, 1035–1050. [[CrossRef](#)]
3. Zhang, Q.; Liang, Y.; Feng, H.; Ma, R.; Tian, Y.; Zhang, J.; Fang, J. A study of oxidative stress induced by non-thermal plasma-activated water for bacterial damage. *Appl. Phys. Lett.* **2013**, *102*, 203701. [[CrossRef](#)]
4. Wong, K.S.; Hung, Y.M.; Tan, M.K. Hybrid treatment via MHz acoustic waves and plasma to enhance seed germination in mung bean. *IEEE Trans. Ultrason. Ferroelectr. Freq. Control* **2021**, *68*, 3438–3445. [[CrossRef](#)] [[PubMed](#)]
5. Low, M.; Sow, W.S.; Hung, Y.M.; Tan, M.K. Increase in Leidenfrost point via plasma-activated water. *Int. J. Therm. Sci.* **2023**, *184*, 107908. [[CrossRef](#)]
6. Low, M.; Hung, Y.M.; Tan, M.K. Cooling enhancement for light-emitting diode using plasma-activated water. *Appl. Therm. Eng.* **2023**, *230*, 120671. [[CrossRef](#)]
7. Chan, J.S.; Low, M.; Poh, P.E.; Yeo, L.Y.; Tan, M.K. Palm oil mill effluent processing via hybrid plasma and acoustic treatment. *J. Water Process. Eng.* **2023**, *51*, 103455. [[CrossRef](#)]
8. Joshi, S.G.; Cooper, M.; Yost, A.; Paff, M.; Ercan, U.K.; Fridman, G.; Friedman, G.; Fridman, A.; Brooks, A.D. Nonthermal Dielectric-Barrier Discharge Plasma-Induced Inactivation Involves Oxidative DNA Damage and Membrane Lipid Peroxidation in *Escherichia coli*. *Antimicrob. Agents Chemother.* **2011**, *55*, 1053–1062. [[CrossRef](#)]
9. Dolezalova, E.; Lukes, P. Membrane damage and active but nonculturable state in liquid cultures of *Escherichia coli* treated with an atmospheric pressure plasma jet. *Bioelectrochemistry* **2015**, *103*, 7–14. [[CrossRef](#)]
10. Li, Y.; Pan, J.; Ye, G.; Zhang, Q.; Wang, J.; Zhang, J.; Fang, J. In Vitro studies of the antimicrobial effect of non-thermal plasma-activated water as a novel mouthwash. *Eur. J. Oral Sci.* **2017**, *125*, 463–470. [[CrossRef](#)]
11. Kashket, E.R. Bioenergetics of lactic acid bacteria: Cytoplasmic pH and osmotolerance. *FEMS Microbiol. Lett.* **1987**, *46*, 233–244. [[CrossRef](#)]
12. Yusupov, M.; Bogaerts, A.; Huygh, S.; Snoeckx, R.; van Duin, A.C.T.; Neyts, E.C. Plasma-Induced Destruction of Bacterial Cell Wall Components: A Reactive Molecular Dynamics Simulation. *J. Phys. Chem. C* **2013**, *117*, 5993–5998. [[CrossRef](#)]
13. Kumar, S.J.; Chintagunta, A.D.; Reddy, Y.M.; Rajjou, L.; Garlapati, V.K.; Agarwal, D.K.; Prasad, S.R.; Simal-Gandara, J. Implications of reactive oxygen and nitrogen species in seed physiology for sustainable crop productivity under changing climate conditions. *Curr. Plant Biol.* **2021**, *26*, 100197. [[CrossRef](#)]
14. Fan, L.; Liu, X.; Ma, Y.; Xiang, Q. Effects of plasma-activated water treatment on seed germination and growth of mung bean sprouts. *J. Taibah Univ. Sci.* **2020**, *14*, 823–830. [[CrossRef](#)]
15. Ndiffo Yemeli, G.B.; Švubová, R.; Kostolani, D.; Kyzek, S.; Machala, Z. The effect of water activated by nonthermal air plasma on the growth of farm plants: Case of maize and barley. *Plasma Process. Polym.* **2021**, *18*, 2000205. [[CrossRef](#)]
16. Islam, S.; Farjana, B.O.; Sajib, S.A.; Nepal, C.R.; Reza, A.; Hasan, M.; Talukder, M.R.; Kabir, A.H. Effects of LPDBD plasma and plasma activated water on germination and growth in rapeseed (*Brassica napus*). *Gesunde Pflanz.* **2019**, *71*, 175–185. [[CrossRef](#)]
17. Chandana, L.; Sangeetha, C.; Shashidhar, T.; Subrahmanyam, C. Non-thermal atmospheric pressure plasma jet for the bacterial inactivation in an aqueous medium. *Sci. Total Environ.* **2018**, *640–641*, 493–500. [[CrossRef](#)]
18. Lukes, P.; Dolezalova, E.; Sisrova, I.; Clupek, M. Aqueous-phase chemistry and bactericidal effects from an air discharge plasma in contact with water: Evidence for the formation of peroxynitrite through a pseudo-second-order post-discharge reaction of H<sub>2</sub>O<sub>2</sub> and HNO<sub>2</sub>. *Plasma Sources Sci. Technol.* **2014**, *23*, 015019. [[CrossRef](#)]
19. Glaze, W.H.; Kang, J.W.; Chapin, D.H. The Chemistry of Water Treatment Processes Involving Ozone, Hydrogen Peroxide and Ultraviolet Radiation. *Ozone Sci. Eng.* **1987**, *9*, 335–352. [[CrossRef](#)]
20. Tarabová, B.; Lukeš, P.; Hammer, M.U.; Jablonowski, H.; von Woedtke, T.; Reuter, S.; Machala, Z. Fluorescence measurements of peroxynitrite/peroxynitrous acid in cold air plasma treated aqueous solutions. *Phys. Chem. Chem. Phys.* **2019**, *21*, 8883–8896. [[CrossRef](#)]
21. Pryor, W.A. Oxy-Radicals and Related Species: Their Formation, Lifetimes, and Reactions. *Annu. Rev. Physiol.* **1986**, *48*, 657–667. [[CrossRef](#)] [[PubMed](#)]
22. Petersen, P.B.; Saykally, R.J. Adsorption of ions to the surface of dilute electrolyte solutions: The Jones-Ray effect revisited. *J. Am. Chem. Soc.* **2005**, *127*, 15446–15452. [[CrossRef](#)] [[PubMed](#)]

23. Weissenborn, P.K.; Pugh, R.J. Surface tension of aqueous solutions of electrolytes: Relationship with ion hydration, oxygen solubility, and bubble coalescence. *J. Colloid Interface Sci.* **1996**, *184*, 550–563. [[CrossRef](#)]
24. Shen, J.; Tian, Y.; Li, Y.; Ma, R.; Zhang, Q.; Zhang, J.; Fang, J. Bactericidal Effects against *S. aureus* and Physicochemical Properties of Plasma Activated Water stored at different temperatures. *Sci. Rep.* **2016**, *6*, 28505. [[CrossRef](#)]
25. Ma, R.; Wang, G.; Tian, Y.; Wang, K.; Zhang, J.; Fang, J. Non-thermal plasma-activated water inactivation of food-borne pathogen on fresh produce. *J. Hazard. Mater.* **2015**, *300*, 643–651. [[CrossRef](#)] [[PubMed](#)]
26. Xu, Y.; Tian, Y.; Ma, R.; Liu, Q.; Zhang, J. Effect of plasma activated water on the postharvest quality of button mushrooms, *Agaricus bisporus*. *Food Chem.* **2016**, *197*, 436–444. [[CrossRef](#)]
27. Pan, J.; Li, Y.L.; Liu, C.M.; Tian, Y.; Yu, S.; Wang, K.L.; Zhang, J.; Fang, J. Investigation of Cold Atmospheric Plasma-Activated Water for the Dental Unit Waterline System Contamination and Safety Evaluation In Vitro. *Plasma Chem. Plasma Process.* **2017**, *37*, 1091–1103. [[CrossRef](#)]
28. Wang, S.; Xu, D.; Qi, M.; Li, B.; Peng, S.; Li, Q.; Zhang, H.; Liu, D. Plasma-Activated Water Promotes Wound Healing by Regulating Inflammatory Responses. *Biophysica* **2021**, *1*, 297–310. [[CrossRef](#)]
29. Xu, D.; Wang, S.; Li, B.; Qi, M.; Feng, R.; Li, Q.; Zhang, H.; Chen, H.; Kong, M.G. Effects of Plasma-Activated Water on Skin Wound Healing in Mice. *Microorganisms* **2020**, *8*, 1091. [[CrossRef](#)]
30. Liedtke, K.R.; Bekeschus, S.; Kaeding, A.; Hackbarth, C.; Kuehn, J.P.; Heidecke, C.D.; von Bernstorff, W.; von Woedtke, T.; Partecke, L.I. Non-thermal plasma-treated solution demonstrates antitumor activity against pancreatic cancer cells In Vitro and In Vivo. *Sci. Rep.* **2017**, *7*, 8319. [[CrossRef](#)]
31. Ranieri, P.; Sponsel, N.; Kizer, J.; Rojas-Pierce, M.; Hernández, R.; Gatiboni, L.; Grunden, A.; Stapelmann, K. Plasma agriculture: Review from the perspective of the plant and its ecosystem. *Plasma Process. Polym.* **2021**, *18*, 2000162. [[CrossRef](#)]
32. Kutasi, K.; Krstulović, N.; Jurov, A.; Salamon, K.; Popović, D.; Milošević, S. Controlling: The composition of plasma-activated water by Cu ions. *Plasma Sources Sci. Technol.* **2021**, *30*, 045015. [[CrossRef](#)]
33. Arda, G.; Hsu, C.I. Preservation of Reactive Species in Frozen Plasma-Activated Water and Enhancement of its Bactericidal Activity Through pH Adjustment. *Plasma Chem. Plasma Process.* **2023**, *43*, 599–618. [[CrossRef](#)]
34. Chew, N.S.; Ooi, C.W.; Yeo, L.Y.; Tan, M.K. Hybrid atmospheric pressure plasma generation and DC electro spray aerosolization of plasma-activated water for surface pathogen disinfection. *Plasma Process. Polym.* **2023**, *20*, 2200128. [[CrossRef](#)]
35. Zhang, Q.; Ma, R.; Tian, Y.; Su, B.; Wang, K.; Yu, S.; Zhang, J.; Fang, J. Sterilization Efficiency of a Novel Electrochemical Disinfectant against *Staphylococcus aureus*. *Environ. Sci. Technol.* **2016**, *50*, 3184–3192. [[CrossRef](#)]
36. Wu, S.; Zhang, Q.; Ma, R.; Yu, S.; Wang, K.; Zhang, J.; Fang, J. Reactive radical-driven bacterial inactivation by hydrogen-peroxide-enhanced plasma-activated-water. *Eur. Phys. J. Spec. Top.* **2017**, *226*, 2887–2899. [[CrossRef](#)]
37. Lukes, P.; Locke, B.R.; Brisset, J.L. Aqueous-Phase Chemistry of Electrical Discharge Plasma in Water and in Gas-Liquid Environments. In *Plasma Chemistry and Catalysis in Gases and Liquids*; Wiley: Hoboken, NJ, USA, 2012; pp. 243–308.
38. Kaushik, N.K.; Ghimire, B.; Li, Y.; Adhikari, M.; Veerana, M.; Kaushik, N.; Jha, N.; Adhikari, B.; Lee, S.J.; Masur, K.; et al. Biological and medical applications of plasma-activated media, water and solutions. *Biol. Chem.* **2018**, *400*, 39–62. [[CrossRef](#)]
39. Gligorovski, S.; Strekowski, R.; Barbati, S.; Vione, D. Environmental Implications of Hydroxyl Radicals ( $\bullet\text{OH}$ ). *Chem. Rev.* **2015**, *115*, 13051–13092. [[CrossRef](#)]
40. Liu, D.X.; Liu, Z.C.; Chen, C.; Yang, A.J.; Li, D.; Rong, M.Z.; Chen, H.L.; Kong, M.G. Aqueous reactive species induced by a surface air discharge: Heterogeneous mass transfer and liquid chemistry pathways. *Sci. Rep.* **2016**, *6*, 23737. [[CrossRef](#)]
41. Kovačević, V.V.; Dojčinović, B.P.; Jović, M.; Roglić, G.M.; Obradović, B.M.; Kuraica, M.M. Measurement of reactive species generated by dielectric barrier discharge in direct contact with water in different atmospheres. *J. Phys. D Appl. Phys.* **2017**, *50*, 155205. [[CrossRef](#)]
42. He, X.; Lin, J.; He, B.; Xu, L.; Li, J.; Chen, Q.; Yue, G.; Xiong, Q.; Liu, Q.H. The formation pathways of aqueous hydrogen peroxide in a plasma-liquid system with liquid as the cathode. *Plasma Sources Sci. Technol.* **2018**, *27*, 085010. [[CrossRef](#)]
43. Niethammer, P.; Grabher, C.; Look, A.T.; Mitchison, T.J. A tissue-scale gradient of hydrogen peroxide mediates rapid wound detection in zebrafish. *Nature* **2009**, *459*, 996–999. [[CrossRef](#)] [[PubMed](#)]
44. Boehm, D.; Curtin, J.; Cullen, P.; Bourke, P. Hydrogen Peroxide and Beyond—the Potential of High-voltage Plasma-activated Liquids Against Cancerous Cells. *Anti-Cancer Agents Med. Chem.* **2018**, *18*, 815–823. [[CrossRef](#)]
45. Kim, Y.H.; Hong, Y.J.; Baik, K.Y.; Kwon, G.C.; Choi, J.J.; Cho, G.S.; Uhm, H.S.; Kim, D.Y.; Choi, E.H. Measurement of Reactive Hydroxyl Radical Species Inside the Biosolutions During Non-thermal Atmospheric Pressure Plasma Jet Bombardment onto the Solution. *Plasma Chem. Plasma Process.* **2014**, *34*, 457–472. [[CrossRef](#)]
46. Adachi, T.; Tanaka, H.; Nonomura, S.; Hara, H.; Kondo, S.-i.; Hori, M. Plasma-activated medium induces A549 cell injury via a spiral apoptotic cascade involving the mitochondrial–nuclear network. *Free. Radic. Biol. Med.* **2015**, *79*, 28–44. [[CrossRef](#)] [[PubMed](#)]
47. Zhou, R.; Zhou, R.; Yu, F.; Xi, D.; Wang, P.; Li, J.; Wang, X.; Zhang, X.; Bazaka, K.; Ostrikov, K.K. Removal of organophosphorus pesticide residues from *Lycium barbarum* by gas phase surface discharge plasma. *Chem. Eng. J.* **2018**, *342*, 401–409. [[CrossRef](#)]
48. Ikawa, S.; Kitano, K.; Hamaguchi, S. Effects of pH on Bacterial Inactivation in Aqueous Solutions due to Low-Temperature Atmospheric Pressure Plasma Application. *Plasma Process. Polym.* **2010**, *7*, 33–42. [[CrossRef](#)]
49. Lu, P.; Boehm, D.; Cullen, P.; Bourke, P. Controlled cytotoxicity of plasma treated water formulated by open-air hybrid mode discharge. *Appl. Phys. Lett.* **2017**, *110*, 264102. [[CrossRef](#)]

50. Girard, P.M.; Arbabian, A.; Fleury, M.; Bauville, G.; Puech, V.; Dutreix, M.; Sousa, J.S. Synergistic effect of H<sub>2</sub>O<sub>2</sub> and NO<sub>2</sub> in cell death induced by cold atmospheric He plasma. *Sci. Rep.* **2016**, *6*, 29098. [[CrossRef](#)]
51. Zhou, R.; Zhang, X.; Bi, Z.; Zong, Z.; Niu, J.; Song, Y.; Liu, D.; Yang, S. Inactivation of *Escherichia coli* Cells in Aqueous Solution by Atmospheric-Pressure N<sub>2</sub>, He, Air, and O<sub>2</sub> Microplasmas. *Appl. Environ. Microbiol.* **2015**, *81*, 5257–5265. [[CrossRef](#)]
52. Zhou, R.; Zhou, R.; Prasad, K.; Fang, Z.; Speight, R.; Bazaka, K.; Ostrikov, K.K. Cold atmospheric plasma activated water as a prospective disinfectant: The crucial role of peroxyxynitrite. *Green Chem.* **2018**, *20*, 5276–5284. [[CrossRef](#)]
53. Bradu, C.; Kutasi, K.; Magureanu, M.; Puač, N.; Živković, S. Reactive nitrogen species in plasma-activated water: Generation, chemistry and application in agriculture. *J. Phys. D Appl. Phys.* **2020**, *53*, 223001. [[CrossRef](#)]
54. Carpenter, A.W.; Schoenfish, M.H. Nitric oxide release: Part II. Therapeutic applications. *Chem. Soc. Rev.* **2012**, *41*, 3742. [[CrossRef](#)] [[PubMed](#)]
55. Verlackt, C.C.W.; Boxem, W.V.; Bogaerts, A. Transport and accumulation of plasma generated species in aqueous solution. *Phys. Chem. Chem. Phys.* **2018**, *20*, 6845–6859. [[CrossRef](#)]
56. Jablonowski, H.; Schmidt-Bleker, A.; Weltmann, K.D.; von Woedtke, T.; Wende, K. Non-touching plasma-liquid interaction—Where is aqueous nitric oxide generated? *Phys. Chem. Chem. Phys.* **2018**, *20*, 25387–25398. [[CrossRef](#)] [[PubMed](#)]
57. Yan, D.; Sherman, J.H.; Cheng, X.; Ratovitski, E.; Canady, J.; Keidar, M. Controlling plasma stimulated media in cancer treatment application. *Appl. Phys. Lett.* **2014**, *105*, 224101. [[CrossRef](#)]
58. Pacher, P.; Beckman, J.S.; Liaudet, L. Nitric Oxide and Peroxynitrite in Health and Disease. *Physiol. Rev.* **2007**, *87*, 315–424. [[CrossRef](#)]
59. Chen, C.; Li, F.; Chen, H.L.; Kong, M.G. Aqueous reactive species induced by a PCB surface micro-discharge air plasma device: A quantitative study. *J. Phys. D Appl. Phys.* **2017**, *50*, 445208. [[CrossRef](#)]
60. Beckman, J.S.; Beckman, T.W.; Chen, J.; Marshall, P.A.; Freeman, B.A. Apparent hydroxyl radical production by peroxyxynitrite: Implications for endothelial injury from nitric oxide and superoxide. *Proc. Natl. Acad. Sci. USA* **1990**, *87*, 1620–1624. [[CrossRef](#)]
61. Zhou, R.; Zhou, R.; Wang, P.; Xian, Y.; Mai-Prochnow, A.; Lu, X.; Cullen, P.; Ostrikov, K.K.; Bazaka, K. Plasma-activated water: Generation, origin of reactive species and biological applications. *J. Phys. D Appl. Phys.* **2020**, *53*, 303001. [[CrossRef](#)]
62. Gao, Y.; Francis, K.; Zhang, X. Review on formation of cold plasma activated water (PAW) and the applications in food and agriculture. *Food Res. Int.* **2022**, *157*, 111246. [[CrossRef](#)] [[PubMed](#)]
63. Hu, X.; Zhang, Y.; Wu, R.A.; Liao, X.; Liu, D.; Cullen, P.J.; Zhou, R.W.; Ding, T. Diagnostic analysis of reactive species in plasma-activated water (PAW): Current advances and outlooks. *J. Phys. D Appl. Phys.* **2021**, *55*, 023002. [[CrossRef](#)]
64. Morabit, Y.; Hasan, M.I.; Whalley, R.D.; Robert, E.; Modic, M.; Walsh, J.L. A review of the gas and liquid phase interactions in low-temperature plasma jets used for biomedical applications. *Eur. Phys. J. D* **2021**, *75*, 32. [[CrossRef](#)]
65. Ghimire, B.; Szili, E.J.; Patenall, B.L.; Lamichhane, P.; Gaur, N.; Robson, A.J.; Trivedi, D.; Thet, N.T.; Jenkins, A.T.A.; Choi, E.H.; et al. Enhancement of hydrogen peroxide production from an atmospheric pressure argon plasma jet and implications to the antibacterial activity of plasma activated water. *Plasma Sources Sci. Technol.* **2021**, *30*, 035009. [[CrossRef](#)]
66. He, L.; He, F.; Ouyang, J.; Dou, W. Effects of electrode gap on radio-frequency discharge characteristics with a hollow electrode. *Phys. Plasmas* **2020**, *27*, 123511. [[CrossRef](#)]
67. Ghimire, B.; Sornsakdanuphap, J.; Hong, Y.J.; Uhm, H.S.; Weltmann, K.D.; Choi, E.H. The effect of the gap distance between an atmospheric-pressure plasma jet nozzle and liquid surface on OH and N<sub>2</sub> species concentrations. *Phys. Plasmas* **2017**, *24*, 073502. [[CrossRef](#)]
68. Ito, T.; Uchida, G.; Nakajima, A.; Takenaka, K.; Setsuhara, Y. Control of reactive oxygen and nitrogen species production in liquid by nonthermal plasma jet with controlled surrounding gas. *Jpn. J. Appl. Phys.* **2016**, *56*, 01AC06. [[CrossRef](#)]
69. Sergeichev, K.F.; Lukina, N.A.; Sarimov, R.M.; Smirnov, I.G.; Simakin, A.V.; Dorokhov, A.S.; Gudkov, S.V. Physicochemical Properties of Pure Water Treated by Pure Argon Plasma Jet Generated by Microwave Discharge in Opened Atmosphere. *Front. Phys.* **2021**, *8*, 614684. [[CrossRef](#)]
70. Lamichhane, P.; Acharya, T.R.; Kaushik, N.; Nguyen, L.N.; Lim, J.S.; Hessel, V.; Kaushik, N.K.; Choi, E.H. Non-thermal argon plasma jets of various lengths for selective reactive oxygen and nitrogen species production. *J. Environ. Chem. Eng.* **2022**, *10*, 107782. [[CrossRef](#)]
71. Wende, K.; Williams, P.; Dalluge, J.; Gaens, W.V.; Aboubakr, H.; Bischof, J.; von Woedtke, T.; Goyal, S.M.; Weltmann, K.D.; Bogaerts, A.; et al. Identification of the biologically active liquid chemistry induced by a nonthermal atmospheric pressure plasma jet. *Biointerphases* **2015**, *10*, 029518. [[CrossRef](#)]
72. Shao, T.; Zhang, C.; Wang, R.; Zhou, Y.; Xie, Q.; Fang, Z. Comparison of Atmospheric-Pressure He and Ar Plasma Jets Driven by Microsecond Pulses. *IEEE Trans. Plasma Sci.* **2014**, *43*, 726–732. [[CrossRef](#)]
73. Vlad, I.E.; Anghel, S.D. Time stability of water activated by different on-liquid atmospheric pressure plasmas. *J. Electrostat.* **2017**, *87*, 284–292. [[CrossRef](#)]
74. Liang, J.; Zhou, X.; Zhao, Z.; Wang, W.; Yang, D.; Yuan, H. Reactive oxygen and nitrogen species in Ar, N<sub>2</sub>, O<sub>2</sub> atmospheric-pressure nanosecond pulsed plasmas in contact with liquid. *Phys. Plasmas* **2019**, *26*, 023521. [[CrossRef](#)]
75. Baik, K.Y.; Kim, Y.H.; Ryu, Y.H.; Kwon, H.S.; Park, G.; Uhm, H.S.; Choi, E.H. Feeding-Gas Effects of Plasma Jets on *Escherichia coli* in Physiological Solutions. *Plasma Process. Polym.* **2013**, *10*, 235–242. [[CrossRef](#)]
76. Kutasi, K.; Popović, D.; Krstulović, N.; Milošević, S. Tuning the composition of plasma-activated water by a surface-wave microwave discharge and a kHz plasma jet. *Plasma Sources Sci. Technol.* **2019**, *28*, 095010. [[CrossRef](#)]

77. Lamichhane, P.; Ghimire, B.; Mumtaz, S.; Paneru, R.; Ki, S.H.; Choi, E.H. Control of hydrogen peroxide production in plasma activated water by utilizing nitrification. *J. Phys. D Appl. Phys.* **2019**, *52*, 265206. [\[CrossRef\]](#)
78. Kim, D.Y.; Kim, S.J.; Joh, H.M.; Chung, T.H. Characterization of an atmospheric pressure plasma jet array and its application to cancer cell treatment using plasma activated medium. *Phys. Plasmas* **2018**, *25*, 073505. [\[CrossRef\]](#)
79. Sobota, A.; Guaitella, O.; Sretenović, G.B.; Krstić, I.B.; Kovačević, V.V.; Obrusník, A.; Nguyen, Y.N.; Zajíčková, L.; Obradović, B.M.; Kuraica, M.M. Electric field measurements in a kHz-driven He jet—The influence of the gas flow speed. *Plasma Sources Sci. Technol.* **2016**, *25*, 065026. [\[CrossRef\]](#)
80. Zhao, Y.M.; Ojha, S.; Burgess, C.; Sun, D.W.; Tiwari, B. Inactivation efficacy and mechanisms of plasma activated water on bacteria in planktonic state. *J. Appl. Microbiol.* **2020**, *129*, 1248–1260. [\[CrossRef\]](#)
81. Baniya, H.B.; Guragain, R.P.; Panta, G.P.; Safaai, S.S.; Dhungana, S.; Qin, G.; Subedi, D.P. Investigation on Parameters of Atmospheric Pressure Plasma Jet by Electrical and Optical Methods. *J. Nepal Phys. Soc.* **2020**, *6*, 50–56. [\[CrossRef\]](#)
82. Chen, Z.; Obenchain, R.; Wirz, R.E. Tiny Cold Atmospheric Plasma Jet for Biomedical Applications. *Processes* **2021**, *9*, 249. [\[CrossRef\]](#)
83. Hou, C.Y.; Kong, T.K.; Lin, C.M.; Chen, H.L. The Effects of Plasma-Activated Water on Heavy Metals Accumulation in Water Spinach. *Appl. Sci.* **2021**, *11*, 5304. [\[CrossRef\]](#)
84. Aktar, A.; Sarmin, S.; Irin, U.A.; Rashid, M.M.; Hasan, M.M.; Talukder, M.R. Plasma Activated Water: Implication as Fungicide, Growth and Yield Stimulator of Potato (*Solanum tuberosum* L.). *Plasma Med.* **2021**, *11*, 31–46. [\[CrossRef\]](#)
85. Yan, D.; Sherman, J.H.; Keidar, M. Cold atmospheric plasma, a novel promising anti-cancer treatment modality. *Oncotarget* **2017**, *8*, 15977–15995. [\[CrossRef\]](#)
86. Feizollahi, E.; Misra, N.; Roopesh, M.S. Factors influencing the antimicrobial efficacy of Dielectric Barrier Discharge (DBD) Atmospheric Cold Plasma (ACP) in food processing applications. *Crit. Rev. Food Sci. Nutr.* **2021**, *61*, 666–689. [\[CrossRef\]](#)
87. Cullen, P.J.; Lalor, J.; Scally, L.; Boehm, D.; Milosavljević, V.; Bourke, P.; Keener, K. Translation of plasma technology from the lab to the food industry. *Plasma Process. Polym.* **2018**, *15*, 1700085. [\[CrossRef\]](#)
88. Yang, J.K.; Cho, C.H.; Kim, J.H.; Seok, D.C.; Yoo, S.; Kang, I.J. Water Surface Plasma Source for Large Area Water Treatment by Using Volume Dielectric Barrier Discharge. *IEEE Trans. Plasma Sci.* **2022**, *50*, 4612–4619. [\[CrossRef\]](#)
89. Ragni, L.; Berardinelli, A.; Iaccheri, E.; Gozzi, G.; Cevoli, C.; Vannini, L. Influence of the electrode material on the decontamination efficacy of dielectric barrier discharge gas plasma treatments towards *Listeria monocytogenes* and *Escherichia coli*. *Innov. Food Sci. Emerg. Technol.* **2016**, *37*, 170–176. [\[CrossRef\]](#)
90. Ozkan, A.; Dufour, T.; Bogaerts, A.; Reniers, F. How do the barrier thickness and dielectric material influence the filamentary mode and CO<sub>2</sub> conversion in a flowing DBD? *Plasma Sources Sci. Technol.* **2016**, *25*, 045016. [\[CrossRef\]](#)
91. Iqbal, M.M.; Turner, M.M. Influence of Gap Spacing between Dielectric Barriers in Atmospheric Pressure Discharges. *Contrib. Plasma Phys.* **2015**, *55*, 444–458. [\[CrossRef\]](#)
92. Miao, H.; Yun, G. The effect of air plasma on sterilization of *Escherichia coli* in dielectric barrier discharge. *Plasma Sci. Technol.* **2012**, *14*, 735.
93. Miao, H.; Yun, G. The sterilization of *Escherichia coli* by dielectric-barrier discharge plasma at atmospheric pressure. *Appl. Surf. Sci.* **2011**, *257*, 7065–7070. [\[CrossRef\]](#)
94. Liao, X.; Xiang, Q.; Liu, D.; Chen, S.; Ye, X.; Ding, T. Lethal and Sublethal Effect of a Dielectric Barrier Discharge Atmospheric Cold Plasma on *Staphylococcus aureus*. *J. Food Prot.* **2017**, *80*, 928–932. [\[CrossRef\]](#)
95. Gao, X.; Zhang, A.; Héroux, P.; Sand, W.; Sun, Z.; Zhan, J.; Wang, C.; Hao, S.; Li, Z.; Li, Z.; et al. Effect of Dielectric Barrier Discharge Cold Plasma on Pea Seed Growth. *J. Agric. Food Chem.* **2019**, *67*, 10813–10822. [\[CrossRef\]](#) [\[PubMed\]](#)
96. Wang, J.; Zhuang, H.; Lawrence, K.; Zhang, J. Disinfection of chicken fillets in packages with atmospheric cold plasma: Effects of treatment voltage and time. *J. Appl. Microbiol.* **2018**, *124*, 1212–1219. [\[CrossRef\]](#) [\[PubMed\]](#)
97. Sarangapani, C.; Misra, N.; Milosavljevic, V.; Bourke, P.; O'Regan, F.; Cullen, P. Pesticide degradation in water using atmospheric air cold plasma. *J. Water Process. Eng.* **2016**, *9*, 225–232. [\[CrossRef\]](#)
98. Morgan, N. Atmospheric pressure dielectric barrier discharge chemical and biological applications. *Int. J. Phys. Sci.* **2009**, *4*, 885–892.
99. Wang, Y.; Huang, J.; Guo, H.; Puyang, C.; Han, J.; Li, Y.; Ruan, Y. Mechanism and process of sulfamethoxazole decomposition with persulfate activated by pulse dielectric barrier discharge plasma. *Sep. Purif. Technol.* **2022**, *287*, 120540. [\[CrossRef\]](#)
100. Berardinelli, A.; Pasquali, F.; Cevoli, C.; Trevisani, M.; Ragni, L.; Mancusi, R.; Manfreda, G. Sanitisation of fresh-cut celery and radicchio by gas plasma treatments in water medium. *Postharvest Biol. Technol.* **2016**, *111*, 297–304. [\[CrossRef\]](#)
101. Neretti, G.; Taglioli, M.; Colonna, G.; Borghi, C.A. Characterization of a dielectric barrier discharge in contact with liquid and producing a plasma activated water. *Plasma Sources Sci. Technol.* **2016**, *26*, 015013. [\[CrossRef\]](#)
102. Ramakers, M.; Michielsen, I.; Aerts, R.; Meynen, V.; Bogaerts, A. Effect of Argon or Helium on the CO<sub>2</sub> Conversion in a Dielectric Barrier Discharge. *Plasma Process. Polym.* **2015**, *12*, 755–763. [\[CrossRef\]](#)
103. Georgescu, N.; Apostol, L.; Gherendi, F. Inactivation of *Salmonella enterica* serovar Typhimurium on egg surface, by direct and indirect treatments with cold atmospheric plasma. *Food Control* **2017**, *76*, 52–61. [\[CrossRef\]](#)
104. Julák, J.; Křířha, V.; Scholtz, V. Corona discharge: A simple method of its generation and study of its bactericidal properties. *Czechoslov. J. Phys.* **2006**, *56*, B1333–B1338. [\[CrossRef\]](#)

105. Zhang, Y.; Zhou, M.; Lei, L. Degradation of 4-chlorophenol in different gas–liquid electrical discharge reactors. *Chem. Eng. J.* **2007**, *132*, 325–333. [[CrossRef](#)]
106. Jiang, B.; Zheng, J.; Qiu, S.; Wu, M.; Zhang, Q.; Yan, Z.; Xue, Q. Review on electrical discharge plasma technology for wastewater remediation. *Chem. Eng. J.* **2014**, *236*, 348–368. [[CrossRef](#)]
107. Scholtz, V.; Julak, J. Plasma Jetlike Point-to-Point Electrical Discharge in Air and Its Bactericidal Properties. *IEEE Trans. Plasma Sci.* **2010**, *38*, 1978–1980. [[CrossRef](#)]
108. Julák, J.; Scholtz, V. Decontamination of human skin by low-temperature plasma produced by cometary discharge. *Clin. Plasma Med.* **2013**, *1*, 31–34. [[CrossRef](#)]
109. Lukeš, P.; Člupek, M.; Babický, V.; Šunka, P.; Skalný, J.D.; Štefečka, M.; Novák, J.; Málková, Z. Erosion of needle electrodes in pulsed corona discharge in water. *Czechoslov. J. Phys.* **2006**, *56*, B916–B924. [[CrossRef](#)]
110. Puertas, E.C.; Dzafic, A.; Coulombe, S. Investigation of the Electrode Erosion in Pin-to-Liquid Discharges and Its Influence on Reactive Oxygen and Nitrogen Species in Plasma-Activated Water. *Plasma Chem. Plasma Process.* **2020**, *40*, 145–167. [[CrossRef](#)]
111. Kim, H.J.; Han, B.; Woo, C.G.; Kim, Y.J.; Park, S.J.; Yoon, J.P. Ozone emission and electrical characteristics of ionizers with different electrode materials, numbers, and diameters. In Proceedings of the 2015 IEEE Industry Applications Society Annual Meeting, Addison, TX, USA, 18–22 October 2015; IEEE: Piscataway, NJ, USA, 2016.
112. Ono, R.; Oda, T. Measurement of hydroxyl radicals in pulsed corona discharge. *J. Electrostat.* **2002**, *55*, 333–342. [[CrossRef](#)]
113. Anderson, C.E.; Cha, N.R.; Lindsay, A.D.; Clark, D.S.; Graves, D.B. The Role of Interfacial Reactions in Determining Plasma-Liquid Chemistry. *Plasma Chem. Plasma Process.* **2016**, *36*, 1393–1415. [[CrossRef](#)]
114. Guan, Y.; Vaddi, R.S.; Aliseda, A.; Novosselov, I. Experimental and numerical investigation of electrohydrodynamic flow in a point-to-ring corona discharge. *Phys. Rev. Fluids* **2018**, *3*, 043701. [[CrossRef](#)]
115. Defoort, E.; Bellanger, R.; Batiot-Dupeyrat, C.; Moreau, E. Ionic wind produced by a DC needle-to-plate corona discharge with a gap of 15 mm. *J. Phys. D Appl. Phys.* **2020**, *53*, 175202. [[CrossRef](#)]
116. Said, H.A.; Nouri, H.; Zebboudj, Y. Effect of air flow on corona discharge in wire-to-plate electrostatic precipitator. *J. Electrostat.* **2015**, *73*, 19–25. [[CrossRef](#)]
117. Wen, Y.Z.; Liu, H.J.; Liu, W.P.; Jiang, X.Z. Degradation of Organic Contaminants in Water by Pulsed Corona Discharge. *Plasma Chem. Plasma Process.* **2005**, *25*, 137–146. [[CrossRef](#)]
118. Los, A.; Ziuzina, D.; Boehm, D.; Cullen, P.J.; Bourke, P. Inactivation Efficacies and Mechanisms of Gas Plasma and Plasma-Activated Water against *Aspergillus flavus* Spores and Biofilms: A Comparative Study. *Appl. Environ. Microbiol.* **2020**, *86*, e02619-19. [[CrossRef](#)]
119. Ki, S.H.; Noh, H.; Ahn, G.R.; Kim, S.H.; Kaushik, N.K.; Choi, E.H.; Lee, G.J. Influence of Nonthermal Atmospheric Plasma-Activated Water on the Structural, Optical, and Biological Properties of *Aspergillus brasiliensis* Spores. *Appl. Sci.* **2020**, *10*, 6378. [[CrossRef](#)]
120. Su, X.; Tian, Y.; Zhou, H.; Li, Y.; Zhang, Z.; Jiang, B.; Yang, B.; Zhang, J.; Fang, J. Inactivation Efficacy of Nonthermal Plasma-Activated Solutions against Newcastle Disease Virus. *Appl. Environ. Microbiol.* **2018**, *84*, e02836-17. [[CrossRef](#)]
121. Chen, Z.; Garcia, G.; Arumugaswami, V.; Wirz, R.E. Cold atmospheric plasma for SARS-CoV-2 inactivation. *Phys. Fluids* **2020**, *32*, 111702. [[CrossRef](#)]
122. Guo, L.; Yao, Z.; Yang, L.; Zhang, H.; Qi, Y.; Gou, L.; Xi, W.; Liu, D.; Zhang, L.; Cheng, Y.; et al. Plasma-activated water: An alternative disinfectant for S protein inactivation to prevent SARS-CoV-2 infection. *Chem. Eng. J.* **2021**, *421*, 127742. [[CrossRef](#)]
123. Wang, Q.; Zhang, Y.; Wu, L.; Niu, S.; Song, C.; Zhang, Z.; Lu, G.; Qiao, C.; Hu, Y.; Yuen, K.Y.; et al. Structural and functional basis of SARS-CoV-2 entry by using human ACE2. *Cell* **2020**, *181*, 894–904. [[CrossRef](#)] [[PubMed](#)]
124. Smet, C.; Govaert, M.; Kyrylenko, A.; Easdani, M.; Walsh, J.L.; Impe, J.F.V. Inactivation of Single Strains of *Listeria monocytogenes* and *Salmonella typhimurium* Planktonic Cells Biofilms with Plasma Activated Liquids. *Front. Microbiol.* **2019**, *10*, 1539. [[CrossRef](#)] [[PubMed](#)]
125. Julák, J.; Scholtz, V.; Kotúčová, S.; Janoušková, O. The persistent microbicidal effect in water exposed to the corona discharge. *Phys. Med.* **2012**, *28*, 230–239. [[CrossRef](#)]
126. Xiao, Z.; Zhou, W.; Zhang, Y. Fungal polysaccharides. In *Pharmacological Advances in Natural Product Drug Discovery*; Elsevier: Amsterdam, The Netherlands, 2020; pp. 277–299.
127. Song, Y.; Fan, X. Cold plasma enhances the efficacy of aerosolized hydrogen peroxide in reducing populations of *Salmonella typhimurium* and *Listeria innocua* on grape tomatoes, apples, cantaloupe and romaine lettuce. *Food Microbiol.* **2020**, *87*, 103391. [[CrossRef](#)] [[PubMed](#)]
128. Joshi, I.; Salvi, D.; Schaffner, D.W.; Karwe, M.V. Characterization of Microbial Inactivation Using Plasma-Activated Water and Plasma-Activated Acidified Buffer. *J. Food Prot.* **2018**, *81*, 1472–1480. [[CrossRef](#)]
129. Xu, Z.; Zhou, X.; Yang, W.; Zhang, Y.; Ye, Z.; Hu, S.; Ye, C.; Li, Y.; Lan, Y.; Shen, J.; et al. In Vitro antimicrobial effects and mechanism of air plasma-activated water on *Staphylococcus aureus* biofilm. *Plasma Process. Polym.* **2020**, *17*, 1900270. [[CrossRef](#)]
130. Baek, K.H.; Yong, H.I.; Yoo, J.H.; Kim, J.W.; Byeon, Y.S.; Lim, J.; Yoon, S.Y.; Ryu, S.; Jo, C. Antimicrobial effects and mechanism of plasma activated fine droplets produced from arc discharge plasma on planktonic *Listeria monocytogenes* and *Escherichia coli* O157:H7. *J. Phys. D Appl. Phys.* **2020**, *53*, 124002. [[CrossRef](#)]
131. Guo, L.; Xu, R.; Gou, L.; Liu, Z.; Zhao, Y.; Liu, D.; Zhang, L.; Chen, H.; Kong, M.G. Mechanism of Virus Inactivation by Cold Atmospheric-Pressure Plasma and Plasma-Activated Water. *Appl. Environ. Microbiol.* **2018**, *84*, e00726-18. [[CrossRef](#)]

132. Kamgang-Youbi, G.; Herry, J.M.; Meylheuc, T.; Brisset, J.L.; Bellon-Fontaine, M.N.; Doubla, A.; Naitali, M. Microbial inactivation using plasma-activated water obtained by gliding electric discharges. *Let. Appl. Microbiol.* **2009**, *48*, 13–18. [[CrossRef](#)]
133. Xiang, Q.; Kang, C.; Zhao, D.; Niu, L.; Liu, X.; Bai, Y. Influence of organic matters on the inactivation efficacy of plasma-activated water against *E. coli* O157:H7 and *S. aureus*. *Food Control* **2019**, *99*, 28–33. [[CrossRef](#)]
134. Xiang, Q.; Kang, C.; Niu, L.; Zhao, D.; Li, K.; Bai, Y. Antibacterial activity and a membrane damage mechanism of plasma-activated water against *Pseudomonas deceptionensis* CM2. *LWT* **2018**, *96*, 395–401. [[CrossRef](#)]
135. Handorf, O.; Pauker, V.I.; Schnabel, U.; Weihe, T.; Freund, E.; Bekeschus, S.; Riedel, K.; Ehlbeck, J. Characterization of Antimicrobial Effects of Plasma-Treated Water (PTW) Produced by Microwave-Induced Plasma (MidiPLexc) on *Pseudomonas fluorescens* Biofilms. *Appl. Sci.* **2020**, *10*, 3118. [[CrossRef](#)]
136. Liao, X.; Su, Y.; Liu, D.; Chen, S.; Hu, Y.; Ye, X.; Wang, J.; Ding, T. Application of atmospheric cold plasma-activated water (PAW) ice for preservation of shrimps (*Metapenaeus ensis*). *Food Control* **2018**, *94*, 307–314. [[CrossRef](#)]
137. Patange, A.; Lu, P.; Boehm, D.; Cullen, P.; Bourke, P. Efficacy of cold plasma functionalised water for improving microbiological safety of fresh produce and wash water recycling. *Food Microbiol.* **2019**, *84*, 103226. [[CrossRef](#)]
138. Wang, J.; Han, R.; Liao, X.; Ding, T. Application of plasma-activated water (PAW) for mitigating methicillin-resistant *Staphylococcus aureus* (MRSA) on cooked chicken surface. *LWT* **2021**, *137*, 110465. [[CrossRef](#)]
139. Han, J.Y.; Song, W.J.; Kang, J.H.; Min, S.C.; Eom, S.; Hong, E.J.; Ryu, S.; Kim, S.b.; Cho, S.; Kang, D.H. Effect of cold atmospheric pressure plasma-activated water on the microbial safety of Korean rice cake. *LWT* **2020**, *120*, 108918. [[CrossRef](#)]
140. Xiang, Q.; Liu, X.; Liu, S.; Ma, Y.; Xu, C.; Bai, Y. Effect of plasma-activated water on microbial quality and physicochemical characteristics of mung bean sprouts. *Innov. Food Sci. Emerg. Technol.* **2019**, *52*, 49–56. [[CrossRef](#)]
141. Liao, X.; Xiang, Q.; Cullen, P.J.; Su, Y.; Chen, S.; Ye, X.; Liu, D.; Ding, T. Plasma-activated water (PAW) and slightly acidic electrolyzed water (SAEW) as beef thawing media for enhancing microbiological safety. *LWT* **2020**, *117*, 108649. [[CrossRef](#)]
142. Zhai, Y.; Liu, S.; Xiang, Q.; Lyu, Y.; Shen, R. Effect of Plasma-Activated Water on the Microbial Decontamination and Food Quality of Thin Sheets of Bean Curd. *Appl. Sci.* **2019**, *9*, 4223. [[CrossRef](#)]
143. Liu, C.; Chen, C.; Jiang, A.; Sun, X.; Guan, Q.; Hu, W. Effects of plasma-activated water on microbial growth and storage quality of fresh-cut apple. *Innov. Food Sci. Emerg. Technol.* **2020**, *59*, 102256. [[CrossRef](#)]
144. Frías, E.; Iglesias, Y.; Alvarez-Ordóñez, A.; Prieto, M.; González-Raurich, M.; López, M. Evaluation of Cold Atmospheric Pressure Plasma (CAPP) and plasma-activated water (PAW) as alternative non-thermal decontamination technologies for tofu: Impact on microbiological, sensorial and functional quality attributes. *Food Res. Int.* **2020**, *129*, 108859. [[CrossRef](#)] [[PubMed](#)]
145. Zhao, Y.M.; Ojha, S.; Burgess, C.M.; Sun, D.W.; Tiwari, B.K. Influence of various fish constituents on inactivation efficacy of plasma-activated water. *Int. J. Food Sci. Technol.* **2020**, *55*, 2630–2641. [[CrossRef](#)]
146. Gavahian, M.; Sheu, F.H.; Tsai, M.J.; Chu, Y.H. The effects of dielectric barrier discharge plasma gas and plasma-activated water on texture, color, and bacterial characteristics of shiitake mushroom. *J. Food Process. Preserv.* **2020**, *44*, e14316. [[CrossRef](#)]
147. Lin, C.M.; Chu, Y.C.; Hsiao, C.P.; Wu, J.S.; Hsieh, C.W.; Hou, C.Y. The Optimization of Plasma-Activated Water Treatments to Inactivate *Salmonella enteritidis* (ATCC 13076) on Shell Eggs. *Foods* **2019**, *8*, 520. [[CrossRef](#)] [[PubMed](#)]
148. Zhao, Y.; Chen, R.; Liu, D.; Wang, W.; Niu, J.; Xia, Y.; Qi, Z.; Zhao, Z.; Song, Y. Effect of Nonthermal Plasma-Activated Water on Quality and Antioxidant Activity of Fresh-Cut Kiwifruit. *IEEE Trans. Plasma Sci.* **2019**, *47*, 4811–4817. [[CrossRef](#)]
149. Kang, C.; Xiang, Q.; Zhao, D.; Wang, W.; Niu, L.; Bai, Y. Inactivation of *Pseudomonas deceptionensis* CM2 on chicken breasts using plasma-activated water. *J. Food Sci. Technol.* **2019**, *56*, 4938–4945. [[CrossRef](#)]
150. Weibrecht, K.; Müller, K.; Leubner-Metzger, G. First off the mark: Early seed germination. *J. Exp. Bot.* **2011**, *62*, 3289–3309. [[CrossRef](#)]
151. Nonogaki, H. Seed germination—The biochemical and molecular mechanisms. *Breed. Sci.* **2006**, *56*, 93–105. [[CrossRef](#)]
152. Han, C.; Yang, P. Studies on the molecular mechanisms of seed germination. *Proteomics* **2015**, *15*, 1671–1679. [[CrossRef](#)]
153. Lutts, S.; Benincasa, P.; Wojtyla, L.; Kubala, S.; Pace, R.; Lechowska, K.; Quinet, M.; Garnczarska, M. Seed priming: New comprehensive approaches for an old empirical technique. In *New Challenges in Seed Biology-Basic and Translational Research Driving Seed Technology*; IntechOpen: London, UK, 2016; Volume 46.
154. El-Maarouf-Bouteau, H. The Seed and the metabolism regulation. *Biology* **2022**, *11*, 168. [[CrossRef](#)]
155. Oliveira, A.L.; Colnaghi, B.G.; Da Silva, E.Z.; Gouvêa, I.R.; Vieira, R.L.; Augusto, P.E.D. Modelling the effect of temperature on the hydration kinetic of adzuki beans (*Vigna angularis*). *J. Food Eng.* **2013**, *118*, 417–420. [[CrossRef](#)]
156. Miano, A.C.; Sabadoti, V.D.; Augusto, P.E.D. Enhancing the hydration process of common beans by ultrasound and high temperatures: Impact on cooking and thermodynamic properties. *J. Food Eng.* **2018**, *225*, 53–61. [[CrossRef](#)]
157. Li, X.; Liu, X.; Hua, Y.; Chen, Y.; Kong, X.; Zhang, C. Effects of water absorption of soybean seed on the quality of soymilk and the release of flavor compounds. *RSC Adv.* **2019**, *9*, 2906–2918. [[CrossRef](#)] [[PubMed](#)]
158. Sharma, N.; Goyal, S.; Alam, T.; Fatma, S.; Chaoruangrit, A.; Niranjana, K. Effect of high pressure soaking on water absorption, gelatinization, and biochemical properties of germinated and non-germinated foxtail millet grains. *J. Cereal Sci.* **2018**, *83*, 162–170. [[CrossRef](#)]
159. Ueno, S.; Shigematsu, T.; Karo, M.; Hayashi, M.; Fujii, T. Effects of high hydrostatic pressure on water absorption of adzuki beans. *Foods* **2015**, *4*, 148–158. [[CrossRef](#)]
160. Awad, T.; Moharram, H.; Shaltout, O.; Asker, D.; Youssef, M. Applications of ultrasound in analysis, processing and quality control of food: A review. *Food Res. Int.* **2012**, *48*, 410–427. [[CrossRef](#)]

161. Mulet, A.; Cárcel, J.; Sanjuan, N.; Bon, J. New food drying technologies-Use of ultrasound. *Food Sci. Technol. Int.* **2003**, *9*, 215–221. [[CrossRef](#)]
162. Miano, A.C.; Ibarz, A.; Augusto, P.E.D. Ultrasound technology enhances the hydration of corn kernels without affecting their starch properties. *J. Food Eng.* **2017**, *197*, 34–43. [[CrossRef](#)]
163. Wong, K.S.; Lee, L.; Yeo, L.Y.; Tan, M.K. Enhancing rate of water absorption in seeds via a miniature surface acoustic wave device. *R. Soc. Open Sci.* **2019**, *6*, 181560. [[CrossRef](#)]
164. Yan, A.; Chen, Z. The control of seed dormancy and germination by temperature, light and nitrate. *Bot. Rev.* **2020**, *86*, 39–75. [[CrossRef](#)]
165. Wojtyła, Ł.; Lechowska, K.; Kubala, S.; Garnczarska, M. Different modes of hydrogen peroxide action during seed germination. *Front. Plant Sci.* **2016**, *7*, 66.
166. Shim, S.I.; Moon, J.C.; Jang, C.S.; Raymer, P.; Kim, W. Effect of potassium nitrate priming on seed germination of seashore paspalum. *HortScience* **2008**, *43*, 2259–2262. [[CrossRef](#)]
167. Yao, X.; Zhou, M.; Ruan, J.; Peng, Y.; Yang, H.; Tang, Y.; Gao, A.; Cheng, J. Pretreatment with H<sub>2</sub>O<sub>2</sub> alleviates the negative impacts of NaCl stress on seed germination of Tartary buckwheat (*Fagopyrum tataricum*). *Plants* **2021**, *10*, 1784. [[CrossRef](#)]
168. Hemalatha, G.; Renugadevi, J.; Eevera, T. Studies on seed priming with hydrogen peroxide for mitigating salt stress in rice. *Int. J. Curr. Microbiol. App. Sci.* **2017**, *6*, 691–695. [[CrossRef](#)]
169. Miransari, M.; Smith, D. Plant hormones and seed germination. *Environ. Exp. Bot.* **2014**, *99*, 110–121. [[CrossRef](#)]
170. Kumar, A.R.; Sivakumar, D. Role of hormones on seed germination—A review. *Agric. Rev.* **2008**, *29*, 281–289.
171. Song, Q.; Cheng, S.; Chen, Z.; Nie, G.; Xu, F.; Zhang, J.; Zhou, M.; Zhang, W.; Liao, Y.; Ye, J. Comparative transcriptome analysis revealing the potential mechanism of seed germination stimulated by exogenous gibberellin in *Fraxinus hupehensis*. *BMC Plant Biol.* **2019**, *19*, 199. [[CrossRef](#)]
172. Koyuncu, F. Breaking seed dormancy in black mulberry (*Morus nigra* L.) by cold stratification and exogenous application of gibberellic acid. *Acta Biol. Cracoviensia Ser. Bot.* **2005**, *47*, 23–26.
173. Thirumdas, R.; Kothakota, A.; Annapure, U.; Siliveru, K.; Blundell, R.; Gatt, R.; Valdramidis, V.P. Plasma activated water (PAW): Chemistry, physico-chemical properties, applications in food and agriculture. *Trends Food Sci. Technol.* **2018**, *77*, 21–31. [[CrossRef](#)]
174. Del Río, L.A. ROS and RNS in plant physiology: An overview. *J. Exp. Bot.* **2015**, *66*, 2827–2837. [[CrossRef](#)]
175. Wang, J.; Cheng, J.H.; Sun, D.W. Enhancement of wheat seed germination, seedling growth and nutritional properties of wheat plantlet juice by plasma activated water. *J. Plant Growth Regul.* **2023**, *42*, 2006–2022. [[CrossRef](#)]
176. Rathore, V.; Tiwari, B.S.; Nema, S.K. Treatment of pea seeds with plasma activated water to enhance germination, plant growth, and plant composition. *Plasma Chem. Plasma Process.* **2022**, *42*, 109–129. [[CrossRef](#)]
177. Than, H.A.Q.; Pham, T.H.; Nguyen, D.K.V.; Pham, T.H.; Khacef, A. Non-thermal plasma activated water for increasing germination and plant growth of *Lactuca sativa* L. *Plasma Chem. Plasma Process.* **2021**, *42*, 73–89. [[CrossRef](#)]
178. Ekanayake, U.M.; Barclay, M.; Seo, D.H.; Park, M.J.; MacLeod, J.; O'Mullane, A.P.; Motta, N.; Shon, H.K.; Ostrikov, K.K. Utilization of plasma in water desalination and purification. *Desalination* **2021**, *500*, 114903. [[CrossRef](#)]
179. Ekanayake, U.M.; Seo, D.H.; Faershteyn, K.; O'Mullane, A.P.; Shon, H.; MacLeod, J.; Golberg, D.; Ostrikov, K.K. Atmospheric-pressure plasma seawater desalination: Clean energy, agriculture, and resource recovery nexus for a blue planet. *Sustain. Mater. Technol.* **2020**, *25*, e00181. [[CrossRef](#)]
180. Kutasi, K.; Bencs, L.; Tóth, Z.; Milošević, S. The role of metals in the deposition of long-lived reactive oxygen and nitrogen species into the plasma-activated liquids. *Plasma Process. Polym.* **2023**, *20*, 2200143. [[CrossRef](#)]
181. Wong, K.S.; Lim, W.T.H.; Ooi, C.W.; Yeo, L.Y.; Tan, M.K. In situ generation of plasma-activated aerosols via surface acoustic wave nebulization for portable spray-based surface bacterial inactivation. *Lab Chip* **2020**, *20*, 1856–1868. [[CrossRef](#)] [[PubMed](#)]
182. Chew, N.S.; Wong, K.S.; Chang, W.S.; Ooi, C.W.; Yeo, L.Y.; Tan, M.K. Nanoscale plasma-activated aerosol generation for in situ surface pathogen disinfection. *Microsyst. Nanoeng.* **2022**, *8*, 41. [[CrossRef](#)]

**Disclaimer/Publisher's Note:** The statements, opinions and data contained in all publications are solely those of the individual author(s) and contributor(s) and not of MDPI and/or the editor(s). MDPI and/or the editor(s) disclaim responsibility for any injury to people or property resulting from any ideas, methods, instructions or products referred to in the content.